Spring 2010

Characterizing near-field circuit board radiation using crossed electric and magnetic dipole sources

Weiping He

Department:

CHARACTERIZING NEAR-FIELD CIRCUIT BOARD RADIATION USING CROSSED ELECTRIC AND MAGNETIC DIPOLE SOURCES

by

WEIPING HE

A THESIS

Presented to the Faculty of the Graduate School of the

MISSOURI UNIVERSITY OF SCIENCE AND TECHNOLOGY

In Partial Fulfillment of the Requirements for the Degree

MASTER OF SCIENCE IN ELECTRICAL ENGINEERING

2010

Approved by

Richard E. DuBroff, Advisor

Daryl Beetner

David J. Pommerenke

James L. Drewniak

ABSTRACT

A method to analyze radiated emissions of electronic components/circuits is presented in this thesis. More specifically the purpose of this approach is to determine an equivalent source model to accurately represent the radiated emissions produced by the circuits and components. The proposed equivalent source model, which is able to predict both electric and magnetic fields at various distances from the device under test, consists of an array of both electric and magnetic dipoles. Each source point includes two electric dipoles orientated in x and y directions and two magnetic dipoles in x and y directions. The value of current associated with each dipole is obtained by extracting data from an HFSS simulation or from near-field scanning. The field components ($E_{x,}\ E_{y,}\ H_{x,}\ H_{y}$) are used to obtain the equivalent source dipole model. The equivalent source dipole model, in turn, is used to predict all six field components ($E_{x,}\ E_{y,}\ E_{z,}\ H_{x,}\ H_{y,}\ H_{z}$) at one or more observation points. The electric and magnetic dipoles are all assumed to be in a common horizontal plane and the length of each dipole is identical. Validation of field predictions from the model is done using full wave simulation (HFSS) and near-field scanning measurements as well.

ACKNOWLEDGMENTS

I would like to express my sincere appreciation to my advisor Dr. DuBroff, for his advice and direction. I learned all aspects of doing research from my advisor. I would like to express my appreciation for the opportunity of being in ESIGELEC, Rouen France while working as an exchange student with Dr. Christian Arcambal and Priscilla Fernandez, a PhD student in IRSEEM-ESIGELEC. Thanks to Dr. Kosbar and Electrical Engineering Department of MST for Teaching Assistantship during my pursuit of MS degree. Thanks for the financial support from MST EMC Lab and ESIGELEC during different period of my study.

I would like to appreciate Dr. Beetner, Dr. Drewniak and Dr. Pommerenke for being on my committee and for their support of my research in the EMC Lab. It has been my privilege to work in EMC Lab and it's a pleasure to acknowledge all the students. I would also like to appreciate Dr. Bélahcène MAZARI, Dr. Anne Louis, Dr. David BAUDRY for their invitation and thanks to Mrs. Cecilia BRUNEL and Mrs. Hélène VINCENT for making the exchange program possible. It's also a pleasure to work with the graduate students in IRSEEM.

Most of all, I appreciate my family for their encouragement and love.

TABLE OF CONTENTS

Page

LIST OF ILLUSTRATIONS

LIST OF TABLES

1. INTRODUCTION

The solution of EMC problems poses many challenges for the designers of high speed digital electronic components and circuit boards. Equivalent source models, including the ones to be described in this thesis, are useful in facilitating the design process. More specifically, this type of model may allow designers to evaluate design alternatives using simulation rather than a process of trial and error involving the construction and evaluation of functioning hardware. Equivalent source models can also allow manufacturers to characterize the behavioral aspects of their products without revealing the detailed inner structure of their products. Other possible advantages might include far field prediction and emissions testing of circuit designs.

Various approaches to modeling radiated emissions have been proposed and the equivalent source model to be presented here is based on the model developed previously at IRSEEM/ESIGELEC in Rouen, France. Their first model, consisting of a set of electric and/or magnetic dipoles located in a horizontal plane, was able to predict radiated emissions based on a comparison between the field predicted by the equivalent source model and the field predicted by a full wave simulation program [1], [2]. While it may be theoretically possible to represent the radiated emissions in terms of a model comprised entirely of electric dipoles or entirely of magnetic dipoles, the simultaneous use of both electric and magnetic dipoles in the model adds a measure redundancy to the measurements and may make the subsequent field prediction less prone to the propagation and growth of errors due to measurement uncertainty [3], [4].

In the present work, the equivalent source model will consist of both electric and magnetic dipole sources acting simultaneously. The principle of superposition [4] assures that the field produced by two impressed equivalent current sources ($\vec{J}$ and $\vec{M}$) acting simultaneously is equal to the sum of the fields produced by each source acting alone. In this case the electrical current density and the magnetic current density will be denoted by $\vec{J}$ and $\vec{M}$ respectively.

The present equivalent source model also differs slightly from the previously developed model in terms of the variable parameters associated with the equivalent source model. In particular the previous model [1] and [2] used the

variables θ_e, θ_m, I_e and I_m to characterize the magnitude and direction of currents associated with dipoles at a fixed set of predefined locations. The angles θ_e and θ_m are actually associated with the orientation of each electric dipole, or magnetic dipole, respectively. In the model considered in this thesis the variables associated with the set of dipoles at predefined locations is denoted by I_{ex}, I_{ey}, I_{mx}, and I_{my}. In this case all of the variables have the same units and can, in theory, be found from an adequate set of data using a single matrix inversion. The ability to specify I_{ex} and I_{ey} independently would also allow the phases associated with currents in these dipoles to be specified independently.

To demonstrate the procedure of the equivalent dipole source modeling, a microstrip hybrid circuit will be used. Full wave simulations are done to obtain both electric and magnetic fields components (x and y) at a single frequency (960 MHz) on a plane located 2mm above the traces. The equivalent dipole sources are constructed by deriving the currents in each dipole. Fields predicted from the dipole sources are compared to those from full wave simulations on a second plane. Near-field scanning measurements are also done to verify the dipole model sources as shown in Figure 1.1. Specifically, the upper left hand corner shows an example of the microstrip hybrid model as entered into a full wave simulation program (HFSS). All three electric field components and all three magnetic field components are simulated over two horizontal planes (A and B). Plane A is 2mm above the microstrip hybrid. Plane B is 5mm above the microstrip hybrid.

As will be shown in the following section, each electric dipole in the electric dipole model is characterized by filamentary electrical currents I_{ex}, I_{ey}. Similarly each magnetic dipole in the magnetic dipole model is characterized by filamentary magnetic currents I_{mx}, I_{my}. Thus starting from the full wave simulation, an equivalent combined electric and magnetic dipole model can be obtained as shown, symbolically, in the left hand center of the figure. In this case, the equivalent dipole model is calculated based on fields distributed over a plane 2mm above the microstrip hybrid.

Starting with the lower left hand corner, the data for constructing the electric and magnetic field dipole model proceeds in a similar manner except that the simulated values of the electric and magnetic field components are now replaced with experimental measurements. As in the full wave simulation approach the experimental measurements are used to infer the electric and magnetic field distributions on the same pair of horizontal planes, located at 2mm above the microstrip hybrid and 5mm above the microstrip hybrid. This experimental method also produces an equivalent dipole model.

In either case (simulation or measurement) the resulting dipole model can be used to predict the fields on plane B. Thus, there are 4 sets of values for the electromagnetic field components on plane B – one set obtained by direct simulation; one set using an equivalent dipole source model where the dipoles are determined from simulated field values; one set using an equivalent dipole source model where the dipoles are obtained from experimental measurements; and one set where the electromagnetic field components on plane B are experimentally measured.

An illustration of the modeling and verification procedure using a microstrip hybrid:

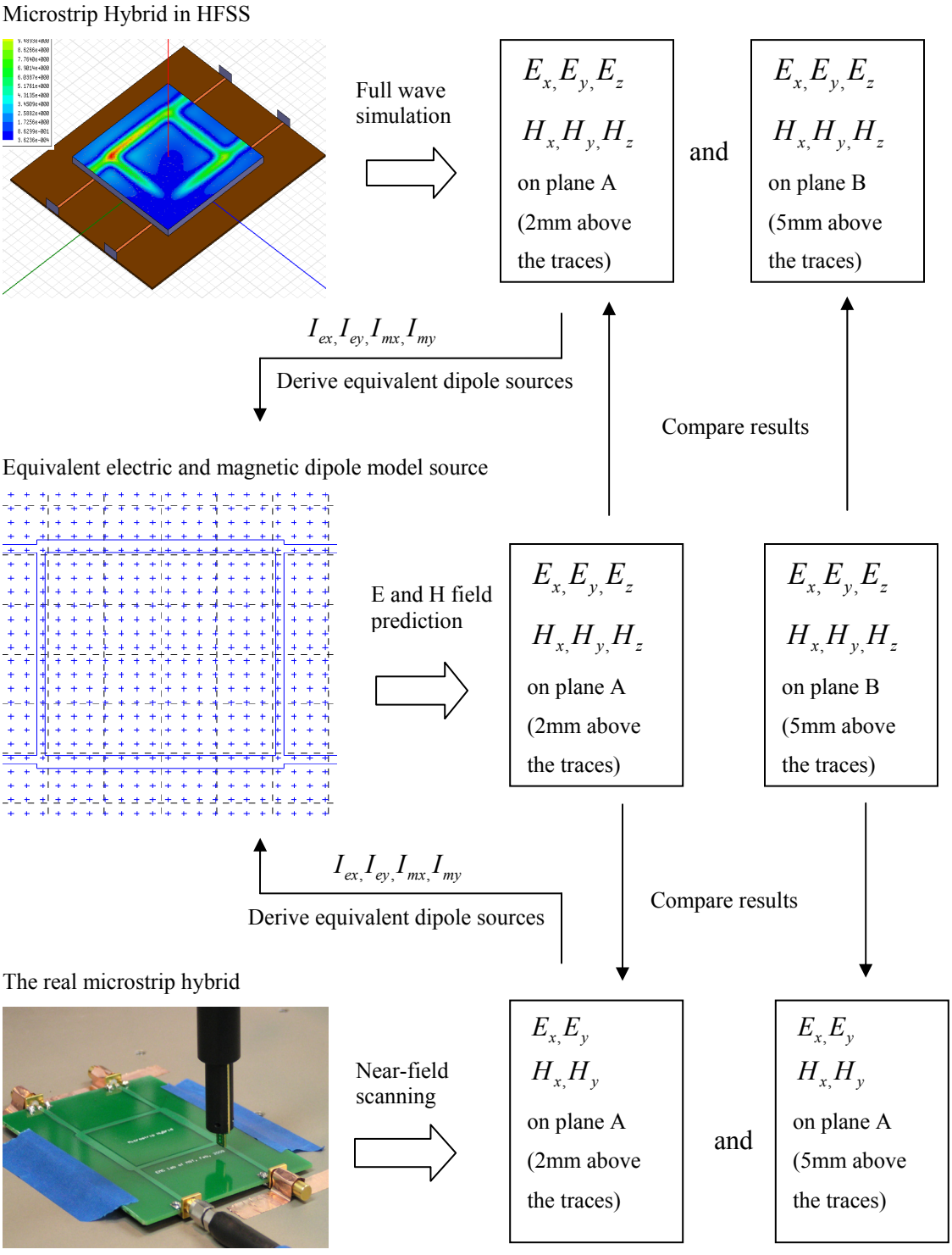

Figure 1.1 Procedure of generating electric and magnetic dipole model source

2. EQUIVALENT RADIATED EMISSION MODEL SOURCE

2.1. INTRODUCTION

Consider a horizontal plane, Π_0, divided into a grid of rectangular cells as shown in Figure 2.1 below:

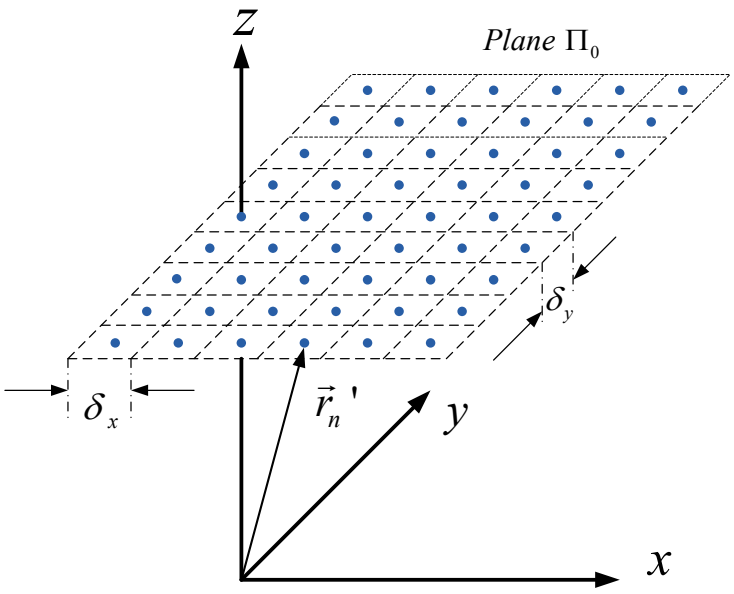

Figure 2.1 A horizontal grid for defining the locations of equivalent crossed dipole sources

The location of the center of the n^{th} cell, as shown in the diagram, is denoted by $\vec{r}_n$ '. Further suppose that there are continuous distributions of electric surface current density $\vec{J}_s(\vec{r})$ and magnetic surface current density $\vec{M}_s(\vec{r})$ defined over this planar surface. Both surface current densities are assumed to be horizontal. The following figure

shows, for example, the electric and magnetic surface current densities at the center of the n^{th} cell.

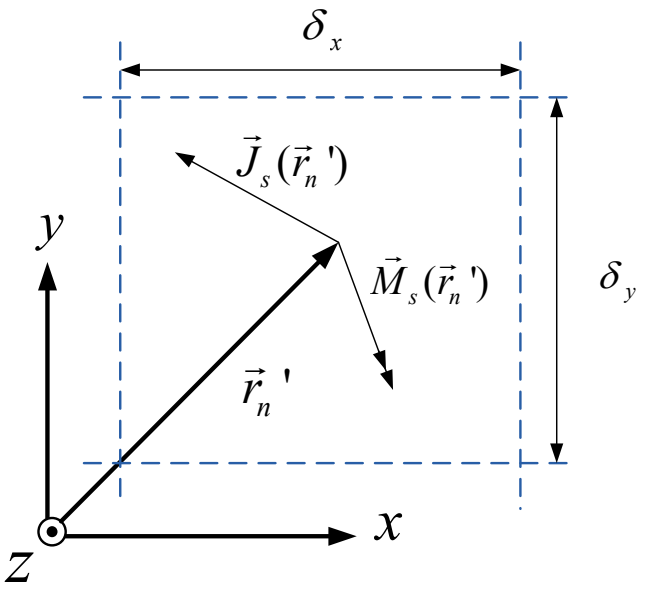

Figure 2.2 Electric and magnetic surface current densities

In the following, it is assumed that the cell is sufficiently small and the surface currents are sufficiently continuous to allow the surface currents to be regarded as being nearly constant over the cell. The continuous surface current densities in the n^{th} cell can be approximated in terms of two filamentary current distributions characterizing the electrical current and an additional two filamentary current distributions characterizing the magnetic current as shown in Figure 2.3.

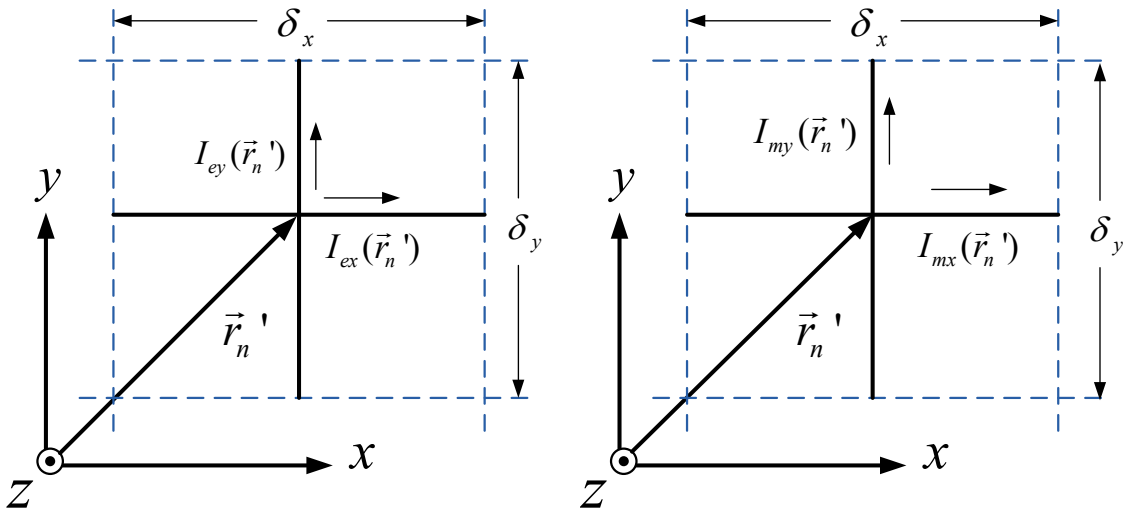

Figure 2.3 Crossed electric and magnetic dipoles

The two electric current filaments form a pair of crossed electric dipoles (as shown on the left) while the two magnetic current filaments form a pair of crossed magnetic dipoles (as shown on the right).

The correspondence between the current distributions in Figure 2.2 and Figure 2.3 is given approximately by

$$\begin{aligned} I_{ex}(\vec{r}_n') &\approx J_{sx}(\vec{r}_n')\delta_y \\ I_{ey}(\vec{r}_n') &\approx J_{sy}(\vec{r}_n')\delta_x \\ I_{mx}(\vec{r}_n') &\approx M_{sx}(\vec{r}_n')\delta_y \\ I_{my}(\vec{r}_n') &\approx M_{sy}(\vec{r}_n')\delta_x \end{aligned} \qquad (2.1)$$

Now consider a second plane, Π_1, parallel to Π_0. This plane contains a set of observation points $\vec{r}_m$. The electric and magnetic crossed dipoles in the plane Π_0 produce an electromagnetic field on Π_1. In general this field will have three electric field components and three magnetic components. However, the relationship between the horizontal components of the electromagnetic field at the observation point $\vec{r}_m$ and the

crossed dipole sources at $\vec{r}_n$ can be written as a set of four simultaneous linear equations, i.e.

$$\begin{bmatrix} E_x(\vec{r}_m) \\ E_y(\vec{r}_m) \\ E_x(\vec{r}_m) \\ E_y(\vec{r}_m) \end{bmatrix} = \Phi(\vec{R}_{mn}) \bullet \begin{bmatrix} I_{ex}(\vec{r}_n{}') \\ I_{ey}(\vec{r}_n{}') \\ I_{mx}(\vec{r}_n{}') \\ I_{my}(\vec{r}_n{}') \end{bmatrix} \tag{2.2}$$

The matrix $\Phi(\vec{R}_{mn})$ is a matrix comprised of four rows and four columns. The sixteen elements of the matrix each depend, in some form, on the magnitude and the direction of the vector $\vec{R}_{mn}$ from the source point $\vec{r}_n{}'$ to the observation point $\vec{r}_m$. Using this notation it is relatively straightforward to generalize to more extensive models. For example if the number of source points is denoted by N and the number of observation points is denoted by M, the system of equations would become

$$\begin{bmatrix} E_x(\vec{r}_1) \\ E_y(\vec{r}_1) \\ H_x(\vec{r}_1) \\ H_y(\vec{r}_1) \\ \vdots \\ E_x(\vec{r}_M) \\ E_y(\vec{r}_M) \\ H_x(\vec{r}_M) \\ H_y(\vec{r}_M) \end{bmatrix} = \begin{bmatrix} \Phi(\vec{R}_{11}) & \cdots & \Phi(\vec{R}_{M1}) \\ \vdots & & \vdots \\ \Phi(\vec{R}_{1N}) & \cdots & \Phi(\vec{R}_{MN}) \end{bmatrix} \begin{bmatrix} I_{ex}(\vec{r}_1') \\ I_{ey}(\vec{r}_1') \\ I_{mx}(\vec{r}_1') \\ I_{my}(\vec{r}_1') \\ \vdots \\ I_{ex}(\vec{r}_N') \\ I_{ey}(\vec{r}_N') \\ I_{mx}(\vec{r}_N') \\ I_{my}(\vec{r}_N') \end{bmatrix} \tag{2.3}$$

In order to obtain the expressions for the matrices, $\Phi(\vec{R}_{mn})$, begin by considering the plane Π_0 to be defined in the xy plane. For simplicity, assume that $\delta_x = \delta_y = l$. Then consider the electromagnetic fields produced by a set of crossed dipoles centered at the origin, i.e. $r' = 0$. Let the observation point be denoted by r_1. In this case, Equation (2.3) reduces to

$$\begin{bmatrix} E_x(\vec{r}_1) \\ E_y(\vec{r}_1) \\ H_x(\vec{r}_1) \\ H_y(\vec{r}_1) \end{bmatrix} = \Phi(\vec{R}_{11}) \begin{bmatrix} I_{ex}(\vec{r}') \\ I_{ey}(\vec{r}') \\ I_{mx}(\vec{r}') \\ I_{my}(\vec{r}') \end{bmatrix}_{\vec{r}'=0} = \begin{bmatrix} \Phi_{11} & \Phi_{12} & \Phi_{13} & \Phi_{14} \\ \Phi_{21} & \Phi_{22} & \Phi_{23} & \Phi_{24} \\ \Phi_{31} & \Phi_{32} & \Phi_{33} & \Phi_{34} \\ \Phi_{41} & \Phi_{42} & \Phi_{43} & \Phi_{44} \end{bmatrix} \begin{bmatrix} I_{ex}(\vec{r}') \\ I_{ey}(\vec{r}') \\ I_{mx}(\vec{r}') \\ I_{my}(\vec{r}') \end{bmatrix}_{\vec{r}'=0} \quad (2.4)$$

The matrix, Φ, is related to the position of the source point and the observation points. The algebraic form and symmetry of these matrix elements will be discussed in a subsequent section. The currents $I_{ex}(\vec{r}')$, $I_{ey}(\vec{r}')$, $I_{mx}(\vec{r}')$, and $I_{my}(\vec{r}')$ represent the equivalent electric and magnetic dipole sources. Once these quantities are found through the solution of a set of simultaneous linear algebraic equations, the resulting electric and magnetic fields at any distance and direction from the source can be found. To accomplish this, the amplitude and phase of the horizontal components of the electric and magnetic field radiated by the electronic device are required. That means, a second plane, A, parallel to Π_0 which contains a set of observation points is needed. This information could be obtained from HFSS simulation or from experimental near-field scanning measurements. The electrical and magnetic fields resulting from equivalent will be compared to the data from simulation and measurements at a third plane B.

The procedure initially requires the auxiliary potential functions $\vec{A}$ and $\vec{F}$ generated, respectively, by $\vec{J}$ and $\vec{M}$ to be expressed in terms of a set of equivalent dipole currents which are used to approximate the electric and magnetic surface currents as previously described in section 1. Then the corresponding electric and magnetic fields are determined ($\vec{E}_{A,}$ $\vec{H}_A$ due to $\vec{A}$ and $\vec{E}_{F,}$ $\vec{H}_F$ due to $\vec{F}$). The total fields are obtained by the superposition of the individual fields due to $\vec{A}$ and $\vec{F}$ ($\vec{J}$ and $\vec{M}$). [5] The net results is a simultaneous linear equations relating the total horizontal electric and magnetic fields to the electric and magnetic currents flowing on a predefined array of crossed electric and crossed magnetic dipoles. By inverting this system of linear equations or by using a least squares approach it is possible to infer a set of dipole currents from a set of known values of the horizontal field components on a horizontal sampling plane. The process is represented schematically in the figure below (Figure 2.4).

Here is an illustration of the method:

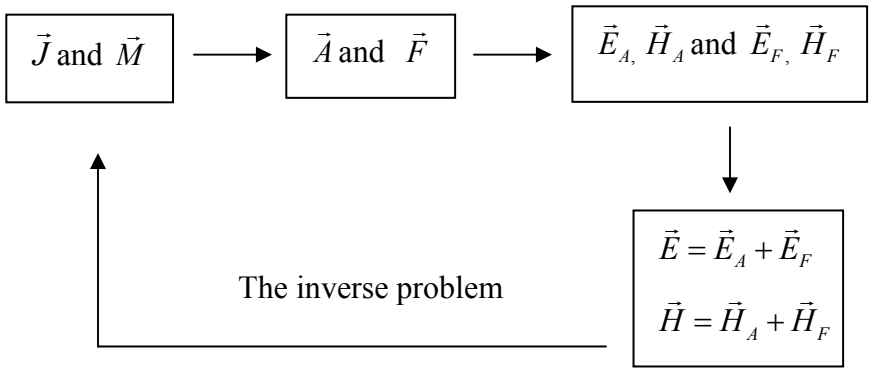

Figure 2.4 Illustration of the method used to generate the equivalent model

Once the currents associated with the equivalent crossed dipole source model have been determined, the entire set of field components can, in theory, be predicted at arbitrary points above the equivalent source model.

The model will be initially developed by evaluating the electric and magnetic fields produced by one set of crossed electric dipole and magnetic dipole located at the origin. The expressions obtained for this case can be readily generalized to apply when the dipoles are located at an arbitrary point.

2.2. FIELDS ASSOCIATED WITH AN ELECTRIC DIPOLE AT ORIGIN

The electrical current associated with an electric dipole source produces a vector magnetic potential, denoted by $\vec{A}$. The electric and magnetic fields produced by the electric dipole source can be found from the vector magnetic potential and these fields will be denoted by $\vec{E}_A$ and $\vec{H}_A$ respectively. Field components in the $\hat{s}$ direction, for example, will be denoted as $\vec{E}_{As}$ and $\vec{H}_{As}$.

2.2.1. The Magnetic Field Produced by an Electric Dipole at the Origin.

Consider an electric dipole at the origin, oriented in the $\hat{s}$ direction as shown in the figure below. In this case $\hat{s}$ is used to denote either horizontal direction ($\hat{x}$ or $\hat{y}$).

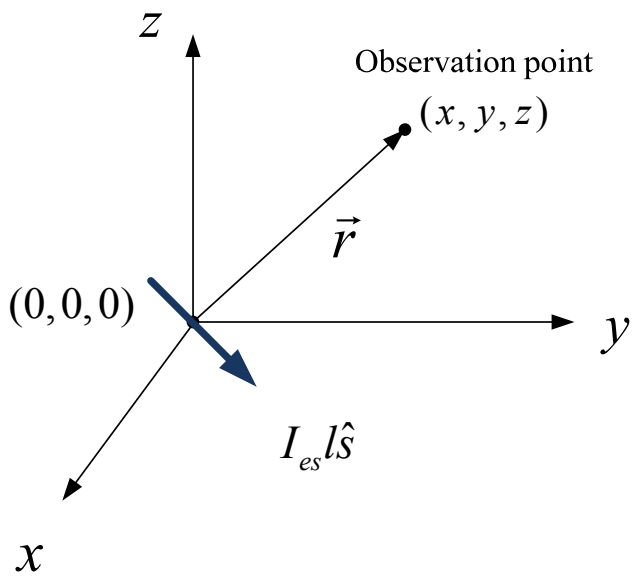

Figure 2.5 An electric dipole at the origin

The vector magnetic potential at the observation point $\vec{r}$ is given by

$$\vec{A}(\vec{r}) = \hat{s}\frac{\mu I_{es} l}{4\pi r} e^{-j\beta r} \qquad (2.5)$$

where $\beta = \omega\sqrt{\mu\varepsilon}$ and where ω is the radian frequency of the time harmonic current source represented by I_{es}. The contribution to the magnetic field $\vec{H}(\vec{r})$ can then be written as

$$\vec{H}_A(\vec{r}) = \frac{1}{\mu}\nabla \times \vec{A}(\vec{r}) = \nabla \times \left(\hat{s}\frac{I_{es} l}{4\pi r} e^{-j\beta r} \right) \qquad (2.6)$$

Using the vector identity for the curl of a vector, $\hat{s}$, times a scalar, $\frac{I_{es} l}{4\pi r} e^{-j\beta r}$ the previous expression becomes

$$\vec{H}_A(\vec{r}) = \nabla\left(\frac{I_{es}l}{4\pi r}e^{-j\beta r}\right)\times\hat{s} + \left(\frac{I_{es}l}{4\pi r}e^{-j\beta r}\right)(\nabla\times\hat{s}) \qquad (2.7)$$

The second term is zero since $\hat{s}$ is a constant. Evaluating the remaining term

$$\begin{aligned}
\vec{H}_A(\vec{r}) &= \nabla\left(\frac{I_{es}l}{4\pi r}e^{-j\beta r}\right)\times\hat{s} = \hat{r}\frac{d}{dr}\left(\frac{I_{es}l}{4\pi r}e^{-j\beta r}\right)\times\hat{s} = \frac{d}{dr}\left(\frac{I_{es}l}{4\pi r}e^{-j\beta r}\right)(\hat{r}\times\hat{s}) \\
&= -\left(\frac{1}{r}+j\beta\right)\left(\frac{I_{es}l}{4\pi r}e^{-j\beta r}\right)(\hat{r}\times\hat{s}) \\
&= \left(\frac{1}{r}+j\beta\right)\left(\frac{I_{es}l}{4\pi r}e^{-j\beta r}\right)(\hat{s}\times\hat{r}) \\
&= \left(\frac{1}{r}+j\beta\right)\left(\frac{I_{es}l}{4\pi r}e^{-j\beta r}\right)\left[\frac{x}{r}(\hat{s}\times\hat{x})+\frac{y}{r}(\hat{s}\times\hat{y})+\frac{z}{r}(\hat{s}\times\hat{z})\right]
\end{aligned} \qquad (2.8)$$

Letting $\hat{s}=\hat{x}$ for electric dipoles oriented in the x direction:

$$\begin{aligned}
\vec{H}_{A_x}(\vec{r}) &= \left(\frac{1}{r}+j\beta\right)\left(\frac{I_{es}l}{4\pi r}e^{-j\beta r}\right)\left[\frac{x}{r}(\hat{x}\times\hat{x})+\frac{y}{r}(\hat{x}\times\hat{y})+\frac{z}{r}(\hat{x}\times\hat{z})\right] \\
&= \left(\frac{1}{r^2}+\frac{j\beta}{r}\right)\left(\frac{I_{ex}l}{4\pi r}e^{-j\beta r}\right)\left[-\hat{y}z+\hat{z}y\right]
\end{aligned} \qquad (2.9)$$

Or, in component form

$$\begin{aligned}
H_{Ax_x} &= 0 \\
H_{Ay_x} &= -\left(\frac{1}{r^2}+\frac{j\beta}{r}\right)\left(\frac{I_{ex}l}{4\pi r}e^{-j\beta r}\right)z \\
H_{Az_x} &= \left(\frac{1}{r^2}+\frac{j\beta}{r}\right)\left(\frac{I_{ex}l}{4\pi r}e^{-j\beta r}\right)y
\end{aligned} \qquad (2.10)$$

The notation $\vec{H}_{As_1\ As_2}$ has been used to represent the $\hat{s}_1$ component of the magnetic field produced by an electric dipole oriented in the $\hat{s}_2$ direction as summarized below

H_{Ax_x}	x component of H field calculated from vector magnetic potential $\vec{A}$ due to the dipole orientated in x direction.
H_{Ay_x}	y component of H field calculated from vector magnetic potential $\vec{A}$ due to the dipole orientated in x direction.
H_{Az_x}	z component of H field calculated from vector magnetic potential $\vec{A}$ due to the dipole orientated in x direction.

Comparing these results with equation (2.4),

$$\begin{aligned}\Phi_{31} &= 0 \\ \Phi_{41} &= -\left(\frac{1}{r^2}+\frac{j\beta}{r}\right)\left(\frac{l}{4\pi r}e^{-j\beta r}\right)z\end{aligned} \tag{2.11}$$

For future use, denote:

$$\Lambda_{21} = \left(\frac{1}{r^2}+\frac{j\beta}{r}\right)\left(\frac{l}{4\pi r}e^{-j\beta r}\right)y \tag{2.12}$$

When the dipole orientation is changed to the y direction, it is found that:

$$\begin{aligned}\vec{H}_{A\_y}(\vec{r}) &= \left(\frac{1}{r}+j\beta\right)\left(\frac{I_{ey}l}{4\pi r}e^{-j\beta r}\right)\left[\frac{x}{r}(\hat{y}\times\hat{x})+\frac{y}{r}(\hat{y}\times\hat{y})+\frac{z}{r}(\hat{y}\times\hat{z})\right] \\ &= \left(\frac{1}{r^2}+\frac{j\beta}{r}\right)\left(\frac{I_{ex}l}{4\pi r}e^{-j\beta r}\right)\left[\hat{x}z-\hat{z}x\right]\end{aligned} \tag{2.13}$$

Or, in component form:

$$\begin{aligned}H_{Ax\_y} &= \left(\frac{1}{r^2}+\frac{j\beta}{r}\right)\left(\frac{I_{ey}l}{4\pi r}e^{-j\beta r}\right)z \\ H_{Ay\_y} &= 0 \\ H_{Az\_y} &= -\left(\frac{1}{r^2}+\frac{j\beta}{r}\right)\left(\frac{I_{ey}l}{4\pi r}e^{-j\beta r}\right)x\end{aligned} \tag{2.14}$$

H_{Ax_y}	x component of H field calculated from vector magnetic potential $\vec{A}$ due to the dipole orientated in y direction.
H_{Ay_y}	y component of H field calculated from vector magnetic potential $\vec{A}$ due to the dipole orientated in y direction.
H_{Az_y}	z component of H field calculated from vector magnetic potential $\vec{A}$ due to the dipole orientated in y direction.

Comparing these results, again, with equation (2.4):

$$\begin{aligned}\Phi_{32} &= \left(\frac{1}{r^2}+\frac{j\beta}{r}\right)\left(\frac{l}{4\pi r}e^{-j\beta r}\right)z \\ \Phi_{42} &= 0 \\ \Lambda_{22} &= \left(\frac{1}{r^2}+\frac{j\beta}{r}\right)\left(\frac{l}{4\pi r}e^{-j\beta r}\right)x\end{aligned} \qquad (2.15)$$

2.2.2. The Electric Field Produced by an Electric Dipole at the Origin.

Starting with Maxwell's curl equations in the frequency domain for a source-free, lossless and homogeneous medium,

$$\nabla\times\vec{H}_A = j\omega\varepsilon\vec{E}_A \qquad (2.16)$$

hence,

$$\vec{E}_A = \frac{1}{j\omega\varepsilon}\nabla\times\vec{H}_A \qquad (2.17)$$

And substituting from equation (2.8)

$$\nabla\times\vec{H}_A(\vec{r}) = \nabla\times\left((\hat{s}\times\hat{r})(\frac{1}{r}+j\beta)(\frac{I_{es}l}{4\pi r}e^{-j\beta r})\right) \qquad (2.18)$$

Again using vector identities, this can be written as

$$\nabla\times\vec{H}_A(\vec{r}) = \nabla\left[(\frac{1}{r}+j\beta)(\frac{I_{es}l}{4\pi r}e^{-j\beta r})\right]\times(\hat{s}\times\hat{r}) + (\frac{1}{r}+j\beta)(\frac{I_{es}l}{4\pi r}e^{-j\beta r})\nabla\times(\hat{s}\times\hat{r})$$

The first term in this expression can be written as

$$\nabla\left[\left(\frac{1}{r}+j\beta\right)\left(\frac{I_{es}l}{4\pi r}e^{-j\beta r}\right)\right]\times(\hat{s}\times\hat{r})=\left\{\left[-\frac{1}{r^2}-\left(\frac{1}{r}+j\beta\right)^2\right]\left(\frac{I_{es}l}{4\pi r}e^{-j\beta r}\right)\right\}\hat{r}\times(\hat{s}\times\hat{r})$$
$$=\left\{\left[\frac{1}{r^2}+\left(\frac{1}{r}+j\beta\right)^2\right]\left(\frac{I_{es}l}{4\pi r}e^{-j\beta r}\right)\right\}\hat{r}\times(\hat{r}\times\hat{s}) \qquad (2.19)$$
$$=\left\{\left[\frac{1}{r^2}+\left(\frac{1}{r}+j\beta\right)^2\right]\left(\frac{I_{es}l}{4\pi r}e^{-j\beta r}\right)\right\}\left[\hat{r}(\hat{r}\cdot\hat{s})-\hat{s}\right]$$

While the second term can be simplified since

$$\nabla\times(\hat{s}\times\hat{r})=\hat{s}(\nabla\cdot\hat{r})-\hat{r}(\nabla\cdot\hat{s})+(\hat{r}\cdot\nabla)\hat{s}-(\hat{s}\cdot\nabla)\hat{r}$$
$$=\hat{s}(\nabla\cdot\hat{r})-(\hat{s}\cdot\nabla)\hat{r}=\frac{2}{r}\hat{s}-\frac{\partial\hat{r}}{\partial s} \qquad (2.20)$$

By noting that $\hat{r}(\nabla\cdot\hat{s})=(\hat{r}\cdot\nabla)\hat{s}=0$, and that $(\hat{s}\cdot\nabla)\cdot\hat{r}$ is simply the directional derivative of $\hat{r}$ in the s direction. In order to combine the two terms in the expression for the curl of $\vec{H}_A$, let $\hat{t}$ be defined as the complement of $\hat{s}$ in the following sense. If $\hat{s}=\hat{x}$ or $\hat{y}$ then $\hat{t}=\hat{y}$ or $\hat{x}$, respectively. Furthermore, let the scalar quantities s and t be defined such that if $\hat{s}=\hat{x}$ or $\hat{y}$ then $s=x$ or y and $t=y$ or x, respectively. Applying this notation to the curl of the magnetic field intensity:

$$
\begin{aligned}
\nabla\times\vec{H}_A(\vec{r}) &= \left\{\left[\frac{1}{r^2}+\left(\frac{1}{r}+j\beta\right)^2\right]\left(\frac{I_{es}l}{4\pi r}e^{-j\beta r}\right)\right\}\left[\hat{r}(\hat{r}\cdot\hat{s})-\hat{s}\right] \\
&+\left(\frac{1}{r}+j\beta\right)\left(\frac{I_{es}l}{4\pi r}e^{-j\beta r}\right)\left(\frac{2}{r}\hat{s}-\frac{\partial\hat{r}}{\partial s}\right) \\
&=\left\{\left[\frac{1}{r^2}+\left(\frac{1}{r}+j\beta\right)^2\right]\left(\frac{I_{es}l}{4\pi r}e^{-j\beta r}\right)\right\}\left\{\hat{s}\left(\frac{s^2}{r^2}-1\right)+\hat{t}\,\frac{st}{r^2}+\hat{z}\,\frac{sz}{r^2}\right\} \\
&+\left(\frac{1}{r}+j\beta\right)\left(\frac{I_{es}l}{4\pi r}e^{-j\beta r}\right)\left(\frac{2}{r}\hat{s}-\frac{\hat{s}}{r}+\frac{(s\hat{s}+t\hat{t}+z\hat{z})s}{r^3}\right) \\
&=\left\{\left[\frac{1}{r^2}+\left(\frac{1}{r}+j\beta\right)^2\right]\left(\frac{I_{es}l}{4\pi r}e^{-j\beta r}\right)\right\}\left\{\hat{s}\left(\frac{s^2}{r^2}-1\right)+\hat{t}\,\frac{st}{r^2}+\hat{z}\,\frac{sz}{r^2}\right\} \\
&+\left(\frac{1}{r}+j\beta\right)\left(\frac{I_{es}l}{4\pi r}e^{-j\beta r}\right)\frac{\hat{s}}{r}+\frac{(s\hat{s}+t\hat{t}+z\hat{z})s}{r^3} \\
&=\left\{\left[\frac{1}{r^2}+\left(\frac{1}{r}+j\beta\right)^2\right]\frac{1}{r^2}+\left(\frac{1}{r}+j\beta\right)^2\right\}\left(\frac{I_{es}l}{4\pi r}e^{-j\beta r}\right)\left\{\hat{s}\left(\frac{s^2}{r^2}-1\right)+\hat{t}\,\frac{st}{r^2}+\hat{z}\,\frac{sz}{r^2}\right\} \\
&+\frac{1}{r^3}\left(\frac{1}{r}+j\beta\right)\left(\frac{I_{es}l}{4\pi r}e^{-j\beta r}\right)\left[\hat{s}(s^2+r^2)+st\hat{t}+sz\hat{z}\right]
\end{aligned}
\tag{2.21}
$$

The s component of the curl of the magnetic field intensity can then be written as

$$
\begin{aligned}
\left[\nabla\times\vec{H}_A(\vec{r})\right]_s &= \left(\frac{I_{es}l}{4\pi r}e^{-j\beta r}\right)\left\{\left[\frac{1}{r^2}+\left(\frac{1}{r}+j\beta\right)^2\right]\left(\frac{s^2}{r^2}-1\right)+\frac{1}{r^3}\left(\frac{1}{r}+j\beta\right)(s^2+r^2)\right\} \\
&=\left(\frac{I_{es}l}{4\pi r}e^{-j\beta r}\right)\left\{\frac{3s^2}{r^3}\left(\frac{1}{r}+j\beta\right)-\frac{1}{r}\left(\frac{1}{r}+j\beta\right)+\beta^2\left(1-\frac{s^2}{r^2}\right)\right\}
\end{aligned}
\tag{2.22}
$$

Now consider the t component:

$$
\begin{aligned}
\left[\nabla\times\vec{H}_A(\vec{r})\right]_t &= \left(\frac{I_{es}l}{4\pi r}e^{-j\beta r}\right)\left\{\left[\frac{1}{r^2}+\left(\frac{1}{r}+j\beta\right)^2\right]\frac{st}{r^2}+\frac{1}{r^3}\left(\frac{1}{r}+j\beta\right)st\right\} \\
&=\left(\frac{I_{es}l}{4\pi r}e^{-j\beta r}\right)\left\{\left[\frac{1}{r^2}+\left(\frac{1}{r}+j\beta\right)^2\right]\frac{1}{r^2}+\frac{1}{r^3}\left(\frac{1}{r}+j\beta\right)\right\}st \\
&=\left(\frac{I_{es}l}{4\pi r}e^{-j\beta r}\right)\left(\frac{3(1+j\beta r)-r^2\beta^2}{r^4}\right)st
\end{aligned}
\tag{2.23}
$$

and the z component becomes the same as the t component after replacing t with z. That is

$$\left[\nabla \times \vec{H}_A(\vec{r})\right]_z = \left(\frac{I_{es} l}{4\pi r} e^{-j\beta r}\right)\left(\frac{3(1+j\beta r) - r^2\beta^2}{r^4}\right) sz \qquad (2.24)$$

From these three equations the electric field components can be obtained as

$$\begin{aligned} E_{As}(\vec{r}) &= \left(\frac{I_{es} l}{4\pi j\omega\varepsilon r} e^{-j\beta r}\right)\left\{\frac{(3s^2 - r^2)}{r^3}\left(\frac{1}{r} + j\beta\right) + \beta^2\left(1 - \frac{s^2}{r^2}\right)\right\} \\ E_{At}(\vec{r}) &= \left(\frac{I_{es} l}{4\pi j\omega\varepsilon r} e^{-j\beta r}\right)\left(\frac{3(1+j\beta r) - r^2\beta^2}{r^4}\right) st \\ E_{Az}(\vec{r}) &= \left(\frac{I_{es} l}{4\pi j\omega\varepsilon r} e^{-j\beta r}\right)\left(\frac{3(1+j\beta r) - r^2\beta^2}{r^4}\right) sz \end{aligned} \qquad (2.25)$$

Now letting $\hat{s} = \hat{x}$:

$$\begin{aligned} \Phi_{11} &= \left(\frac{l}{4\pi j\omega\varepsilon r} e^{-j\beta r}\right)\left\{\frac{(3x^2 - r^2)}{r^3}\left(\frac{1}{r} + j\beta\right) + \beta^2\left(1 - \frac{x^2}{r^2}\right)\right\} \\ \Phi_{21} &= \left(\frac{l}{4\pi j\omega\varepsilon r} e^{-j\beta r}\right)\left(\frac{3(1+j\beta r) - r^2\beta^2}{r^4}\right) xy \\ \Lambda_{11} &= \left(\frac{l}{4\pi j\omega\varepsilon r} e^{-j\beta r}\right)\left(\frac{3(1+j\beta r) - r^2\beta^2}{r^4}\right) xz \end{aligned} \qquad (2.26)$$

While letting $\hat{s} = \hat{y}$ results in:

$$\begin{aligned} \Phi_{12} &= \left(\frac{l}{4\pi j\omega\varepsilon r} e^{-j\beta r}\right)\left(\frac{3(1+j\beta r) - r^2\beta^2}{r^4}\right) yx \\ \Phi_{22} &= \left(\frac{l}{4\pi j\omega\varepsilon r} e^{-j\beta r}\right)\left\{\frac{(3x^2 - r^2)}{r^3}\left(\frac{1}{r} + j\beta\right) + \beta^2\left(1 - \frac{y^2}{r^2}\right)\right\} \\ \Lambda_{12} &= \left(\frac{l}{4\pi j\omega\varepsilon r} e^{-j\beta r}\right)\left(\frac{3(1+j\beta r) - r^2\beta^2}{r^4}\right) yz \end{aligned} \qquad (2.27)$$

2.3. FIELDS ASSOCIATED WITH A MAGNETIC DIPOLE AT ORIGIN

Consider a single horizontal magnetic dipole located at $\vec{r}\,'$ in the xy plane. Let the dipole have a length of l and an orientation in the $\hat{s}$ direction, where the unit vector $\hat{s}$ as previously noted could be parallel to either the x or y axes.

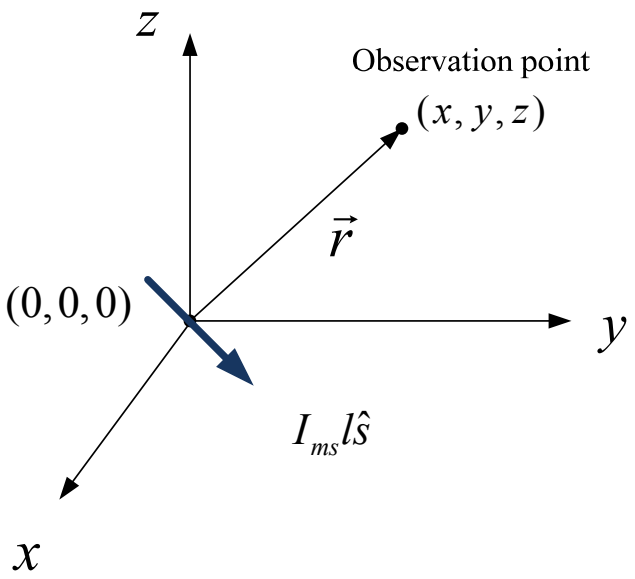

Figure 2.6 A magnetic dipole at the origin

The corresponding vector electric potential is given by

$$\vec{F}(\vec{r}) = \hat{s}\frac{\varepsilon I_{ms} l e^{-j\beta r}}{4\pi r} \qquad (2.28)$$

and the corresponding magnetic field components can be determined as follows

$$\vec{E}_F = -\frac{1}{\varepsilon}\nabla \times \vec{F} \qquad (2.29)$$

Noting the similarity of equation (2.28) and (2.29) with equation (2.5) and (2.29), it is evident that these two pairs of equations are related through duality. Thus knowing the

solutions to one set, (2.5) and (2.6) for example, the solution to the other set (2.28) and (2.29) can be formed by a proper interchange of quantities. [6] The dual equations and dual quantities are listed below:

Table 2.1 Dual equations and dual quantities

Electric Sources (J ≠ 0, M = 0)	Magnetic Sources(J = 0, M ≠ 0)
$\vec{A}(\vec{r}) = \hat{s}\frac{\mu I_{es} l e^{-jkr}}{4\pi r}$	$\vec{F}(\vec{r}) = \hat{s}\frac{\varepsilon I_{ms} l e^{-jkr}}{4\pi r}$
$\vec{H}_A = \frac{1}{\mu}\nabla \times \vec{A}$	$\vec{E}_F = -\frac{1}{\varepsilon}\nabla \times \vec{F}$
$\vec{E}_A = \frac{1}{j\omega\varepsilon}\nabla \times \vec{H}_A$	$\vec{H}_F = \frac{1}{j\omega\varepsilon}\nabla \times \vec{E}_F$
E_A	H_F
H_A	$-E_F$
J	M
A	F
ε	μ
μ	ε
β	β

Using the precious obtained expressions for the fields due to electric sources, this table will allow the corresponding expressions for magnetic sources to be written by inspection.

2.3.1. The Magnetic Field Produced by a Magnetic Dipole at the Origin. Here are the field components of magnetic field due to $\vec{F}$:

$$
\begin{aligned}
H_{Fs}(\vec{r}) &= \left(\frac{I_{ms}l}{4\pi j\omega\mu r}e^{-j\beta r}\right)\left\{\frac{(3s^2-r^2)}{r^3}\left(\frac{1}{r}+j\beta\right)+\beta^2\left(1-\frac{s^2}{r^2}\right)\right\} \\
H_{Ft}(\vec{r}) &= \left(\frac{I_{ms}l}{4\pi j\omega\mu r}e^{-j\beta r}\right)\left(\frac{3(1+j\beta r)-r^2\beta^2}{r^4}\right)st \\
H_{Fz}(\vec{r}) &= \left(\frac{I_{ms}l}{4\pi j\omega\mu r}e^{-j\beta r}\right)\left(\frac{3(1+j\beta r)-r^2\beta^2}{r^4}\right)sz
\end{aligned}
\tag{2.30}
$$

Letting $\hat{s}=\hat{x}$ yields,

$$
\begin{aligned}
\Phi_{33} &= \left(\frac{l}{4\pi j\omega\mu r}e^{-j\beta r}\right)\left\{\frac{(3x^2-r^2)}{r^3}\left(\frac{1}{r}+j\beta\right)+\beta^2\left(1-\frac{x^2}{r^2}\right)\right\} \\
\Phi_{43} &= \left(\frac{l}{4\pi j\omega\mu r}e^{-j\beta r}\right)\left(\frac{3(1+j\beta r)-r^2\beta^2}{r^4}\right)xy \\
\Lambda_{23} &= \left(\frac{l}{4\pi j\omega\mu r}e^{-j\beta r}\right)\left(\frac{3(1+j\beta r)-r^2\beta^2}{r^4}\right)xz
\end{aligned}
\tag{2.31}
$$

While letting $\hat{s}=\hat{y}$ yields,

$$
\begin{aligned}
\Phi_{34} &= \left(\frac{l}{4\pi j\omega\mu r}e^{-j\beta r}\right)\left(\frac{3(1+j\beta r)-r^2\beta^2}{r^4}\right)yx \\
\Phi_{44} &= \left(\frac{l}{4\pi j\omega\mu r}e^{-j\beta r}\right)\left\{\frac{(3y^2-r^2)}{r^3}\left(\frac{1}{r}+j\beta\right)+\beta^2\left(1-\frac{y^2}{r^2}\right)\right\} \\
\Lambda_{24} &= \left(\frac{l}{4\pi j\omega\mu r}e^{-j\beta r}\right)\left(\frac{3(1+j\beta r)-r^2\beta^2}{r^4}\right)yz
\end{aligned}
\tag{2.32}
$$

2.3.2. The Electric Field Produced by a Magnetic Dipole at the Origin. The components of the electric field due to a magnetic dipole at the origin are given by:

$$
\begin{aligned}
E_{Fx\_x} &= 0 \\
E_{Fy\_x} &= -\left(\frac{1}{r^2}+\frac{j\beta}{r}\right)\left(\frac{I_{mx}l}{4\pi r}e^{-j\beta r}\right)z \\
E_{Fz\_x} &= -\left(\frac{1}{r^2}+\frac{j\beta}{r}\right)\left(\frac{I_{mx}l}{4\pi r}e^{-j\beta r}\right)y
\end{aligned}
\tag{2.33}
$$

E_{Fx_x}	x component of E field calculated from vector electric potential $\vec{F}$ due to the dipole orientated in x direction.
E_{Fy_x}	y component of E field calculated from vector magnetic potential $\vec{F}$ due to the dipole orientated in x direction.
E_{Fz_x}	z component of E field calculated from vector magnetic potential $\vec{F}$ due to the dipole orientated in x direction.

$$
\begin{aligned}
E_{Fx\_y} &= -\left(\frac{1}{r^2}+\frac{j\beta}{r}\right)\left(\frac{I_{my}l}{4\pi r}e^{-j\beta r}\right)z \\
E_{Fy\_y} &= 0 \\
E_{Fz\_y} &= \left(\frac{1}{r^2}+\frac{j\beta}{r}\right)\left(\frac{I_{my}l}{4\pi r}e^{-j\beta r}\right)x
\end{aligned}
\qquad (2.34)
$$

E_{Fx_y}	x component of E field calculated from vector electric potential $\vec{F}$ due to the dipole orientated in y direction.
E_{Fy_y}	y component of E field calculated from vector magnetic potential $\vec{F}$ due to the dipole orientated in y direction.
E_{Fz_y}	z component of E field calculated from vector magnetic potential $\vec{F}$ due to the dipole orientated in y direction.

Comparing these expressions with the matrix elements in equation (2.4),

$$
\begin{aligned}
\Phi_{13} &= 0 \\
\Phi_{14} &= -\left(\frac{1}{r^2}+\frac{j\beta}{r}\right)\left(\frac{l}{4\pi r}e^{-j\beta r}\right)z \\
\Lambda_{13} &= -\left(\frac{1}{r^2}+\frac{j\beta}{r}\right)\left(\frac{l}{4\pi r}e^{-j\beta r}\right)y \\
\Phi_{23} &= -\left(\frac{1}{r^2}+\frac{j\beta}{r}\right)\left(\frac{l}{4\pi r}e^{-j\beta r}\right)z \\
\Phi_{24} &= 0 \\
\Lambda_{14} &= \left(\frac{1}{r^2}+\frac{j\beta}{r}\right)\left(\frac{l}{4\pi r}e^{-j\beta r}\right)x
\end{aligned}
\qquad (2.35)
$$

2.4. OBTAIN THE CURRENT IN A SET OF ELECTRIC AND MAGNETIC DIPOLES

In the previous sections the equivalent sources were assumed to be located at the origin while the observed fields were assumed to be at an arbitrary observation point denoted by $\vec{r} = x\hat{x} + y\hat{y} + z\hat{z}$. Under these circumstances, the currents associated with the electric and magnetic dipole can be related to the observed field components through

$$\left[\begin{matrix} I_{ex}(\vec{r}') \\ I_{ey}(\vec{r}') \\ I_{mx}(\vec{r}') \\ I_{my}(\vec{r}') \end{matrix}\right]_{\vec{r}'=0} = \left[\begin{matrix} \Phi_{11} & \Phi_{12} & \Phi_{13} & \Phi_{14} \\ \Phi_{21} & \Phi_{22} & \Phi_{23} & \Phi_{24} \\ \Phi_{31} & \Phi_{32} & \Phi_{33} & \Phi_{34} \\ \Phi_{41} & \Phi_{42} & \Phi_{43} & \Phi_{44} \end{matrix}\right]^{-1} \left[\begin{matrix} E_x(\vec{r}_1) \\ E_y(\vec{r}_1) \\ H_x(\vec{r}_1) \\ H_y(\vec{r}_1) \end{matrix}\right] \tag{2.36}$$

Now consider there are N source points located at $\vec{r}_n$ for $n = 1 \text{ to } N$ and M observation points located at $\vec{r}_m$, for $m = 1 \text{ to } M$. Provided that $M = N$ equation (2.36) can be generalized to

$$\left[\begin{matrix} I_{ex}(\vec{r}_1^{\,'}) \\ I_{ey}(\vec{r}_1^{\,'}) \\ I_{mx}(\vec{r}_1^{\,'}) \\ I_{my}(\vec{r}_1^{\,'}) \\ \vdots \\ I_{ex}(\vec{r}_N^{\,'}) \\ I_{ey}(\vec{r}_N^{\,'}) \\ I_{mx}(\vec{r}_N^{\,'}) \\ I_{my}(\vec{r}_N^{\,'}) \end{matrix}\right] = \left[\begin{matrix} \Phi(\vec{R}_{11}) & \cdots & \Phi(\vec{R}_{M1}) \\ \vdots & & \vdots \\ \Phi(\vec{R}_{1N}) & \cdots & \Phi(\vec{R}_{MN}) \end{matrix}\right]^{-1} \left[\begin{matrix} E_x(\vec{r}_1) \\ E_y(\vec{r}_1) \\ H_x(\vec{r}_1) \\ H_y(\vec{r}_1) \\ \vdots \\ E_x(\vec{r}_M) \\ E_y(\vec{r}_M) \\ H_x(\vec{r}_M) \\ H_y(\vec{r}_M) \end{matrix}\right] \tag{2.37}$$

For the case when the number of observation points exceeds the number of source points the matrix inversion in equation (2.37) can be replaced with the method of least squares. The sixteen element sub matrix, $\Phi(\vec{R}_{MN})$ for $m = 1 \text{ to } M$ and $n = 1 \text{ to } N$ connects the dipole currents at $\vec{r}_n^{\,'}$ to the horizontal field components at $\vec{r}_m$ and has the general form of

$$\begin{bmatrix} \Phi_{11}(\vec{R}_{mn}) & \Phi_{12}(\vec{R}_{mn}) & \Phi_{13}(\vec{R}_{mn}) & \Phi_{14}(\vec{R}_{mn}) \\ \Phi_{21}(\vec{R}_{mn}) & \Phi_{22}(\vec{R}_{mn}) & \Phi_{23}(\vec{R}_{mn}) & \Phi_{24}(\vec{R}_{mn}) \\ \Phi_{31}(\vec{R}_{mn}) & \Phi_{32}(\vec{R}_{mn}) & \Phi_{33}(\vec{R}_{mn}) & \Phi_{34}(\vec{R}_{mn}) \\ \Phi_{41}(\vec{R}_{mn}) & \Phi_{42}(\vec{R}_{mn}) & \Phi_{43}(\vec{R}_{mn}) & \Phi_{44}(\vec{R}_{mn}) \end{bmatrix} \tag{2.38}$$

where $\vec{R}_{mn} = \vec{r}_m - \vec{r}_n^{'} = (x_m - x_n^{'})\hat{x} + (y_m - y_n^{'})\hat{y} + (z_m - z_n^{'})\hat{z}$ to accommodate the shift in the location of the source point from the origin to an arbitrary source point $\vec{r}_n^{'}$.

Then defining

$$\begin{aligned} x_{mn} &= x_m - x_n^{'} \\ y_{mn} &= y_m - y_n^{'} \\ z_{mn} &= z_m - z_n^{'} \\ r_{mn} &= \sqrt{x_{mn}^2 + y_{mn}^2 + z_{mn}^2} \end{aligned} \tag{2.39}$$

The matrix elements of $\Phi(\vec{R}_{MN})$ can be obtained from the matrix elements found for a single source point located at the origin by replacing r with r_{mn}; replacing x with x_{mn}; replacing y with y_{mn}; replacing z with z_{mn}.

It should be noted, however, that the matrix $\Phi(\vec{R}_{MN})$ only expresses the horizontal electromagnetic field components at the observation point $\vec{r}_m$, in terms of the electric and magnetic dipole sources at the source pint, $\vec{r}_n^{'}$. In order to include the contribution to the vertical electric and magnetic fields at the observation point in the matrix $\Phi(\vec{R}_{MN})$ should be replaced with the matrix $\Lambda(\vec{R}_{mn})$ where

$$\Lambda(\vec{R}_{mn}) = \begin{bmatrix} \Phi_{11}(\vec{R}_{mn}) & \Phi_{12}(\vec{R}_{mn}) & \Phi_{13}(\vec{R}_{mn}) & \Phi_{14}(\vec{R}_{mn}) \\ \Phi_{21}(\vec{R}_{mn}) & \Phi_{22}(\vec{R}_{mn}) & \Phi_{23}(\vec{R}_{mn}) & \Phi_{24}(\vec{R}_{mn}) \\ \Lambda_{11}(\vec{R}_{mn}) & \Lambda_{12}(\vec{R}_{mn}) & \Lambda_{13}(\vec{R}_{mn}) & \Lambda_{14}(\vec{R}_{mn}) \\ \Phi_{31}(\vec{R}_{mn}) & \Phi_{32}(\vec{R}_{mn}) & \Phi_{33}(\vec{R}_{mn}) & \Phi_{34}(\vec{R}_{mn}) \\ \Phi_{41}(\vec{R}_{mn}) & \Phi_{42}(\vec{R}_{mn}) & \Phi_{43}(\vec{R}_{mn}) & \Phi_{44}(\vec{R}_{mn}) \\ \Lambda_{21}(\vec{R}_{mn}) & \Lambda_{22}(\vec{R}_{mn}) & \Lambda_{23}(\vec{R}_{mn}) & \Lambda_{24}(\vec{R}_{mn}) \end{bmatrix} \tag{2.40}$$

In summary the matrix elements for both $\Phi(\vec{R}_{MN})$ and $\Lambda(\vec{R}_{mn})$ can be written as

$$\Phi_{11}\left(\vec{R}_{mn}\right)=\left(\frac{l}{4\pi j\omega\varepsilon r_{mn}}\right)\left\{\frac{\left[3x_{mn}^{2}-r_{mn}{}^{2}\right]}{r_{mn}{}^{3}}\left(\frac{1}{r_{mn}}+j\beta\right)+\beta^{2}\left(1-\frac{x_{mn}^{2}}{r_{mn}{}^{2}}\right)\right\}\exp(-j\beta r_{mn})$$

$$\Phi_{12}\left(\vec{R}_{mn}\right)=\Phi_{21}\left(\vec{R}_{mn}\right)=\left(\frac{l}{4\pi j\omega\varepsilon r_{mn}}\right)\left(\frac{3(1+j\beta r_{mn})-r_{mn}{}^{2}\beta^{2}}{r_{mn}{}^{4}}\right)x_{mn}y_{mn}\exp(-j\beta r_{mn})$$

$$\Phi_{13}\left(\vec{R}_{mn}\right)=\Phi_{14}\left(\vec{R}_{mn}\right)=\Phi_{31}\left(\vec{R}_{mn}\right)=\Phi_{42}\left(\vec{R}_{mn}\right)=0$$

$$\Phi_{14}\left(\vec{R}_{mn}\right)=\Phi_{41}\left(\vec{R}_{mn}\right)=-\Phi_{23}\left(\vec{R}_{mn}\right)=-\Phi_{32}\left(\vec{R}_{mn}\right)=\left(\frac{1}{r_{mn}{}^{2}}+\frac{j\beta}{r_{mn}}\right)\left(\frac{l}{4\pi r_{mn}}\right)z_{mn}\exp(-j\beta r_{mn})$$

$$\Lambda_{11}\left(\vec{R}_{mn}\right)=\left(\frac{l}{4\pi j\omega\varepsilon r_{mn}}\right)\left(\frac{3(1+j\beta r_{mn})-r_{mn}{}^{2}\beta^{2}}{r_{mn}{}^{4}}\right)x_{mn}z_{mn}\exp(-j\beta r_{mn})$$

$$\Phi_{22}\left(\vec{R}_{mn}\right)=\left(\frac{l}{4\pi j\omega\varepsilon r_{mn}}\right)\left\{\frac{\left[3x_{mn}^{2}-r_{mn}{}^{2}\right]}{r_{mn}{}^{3}}\left(\frac{1}{r_{mn}}+j\beta\right)+\beta^{2}\left(1-\frac{y_{mn}^{2}}{r_{mn}{}^{2}}\right)\right\}\exp(-j\beta r_{mn})$$

$$\Lambda_{12}\left(\vec{R}_{mn}\right)=\left(\frac{l}{4\pi j\omega\varepsilon r_{mn}}\right)\left(\frac{3(1+j\beta r_{mn})-r_{mn}{}^{2}\beta^{2}}{r_{mn}{}^{4}}\right)y_{mn}z_{mn}\exp(-j\beta r_{mn})$$

$$\Lambda_{13}\left(\vec{R}_{mn}\right)=-\Lambda_{21}\left(\vec{R}_{mn}\right)=-\left(\frac{1}{r_{mn}{}^{2}}+\frac{j\beta}{r_{mn}}\right)\left(\frac{l}{4\pi r_{mn}}\right)y_{mn}\exp(-j\beta r_{mn})$$

$$\Lambda_{14}\left(\vec{R}_{mn}\right)=-\Lambda_{22}\left(\vec{R}_{mn}\right)=\left(\frac{1}{r_{mn}{}^{2}}+\frac{j\beta}{r_{mn}}\right)\left(\frac{l}{4\pi r_{mn}}\right)x_{mn}\exp(-j\beta r_{mn})$$

$$\Phi_{33}\left(\vec{R}_{mn}\right)=\left(\frac{l}{4\pi j\omega\mu r_{mn}}\right)\left\{\frac{\left[3x_{mn}^{2}-r_{mn}{}^{2}\right]}{r_{mn}{}^{3}}\left(\frac{1}{r_{mn}}+j\beta\right)+\beta^{2}\left(1-\frac{x_{mn}^{2}}{r_{mn}{}^{2}}\right)\right\}\exp(-j\beta r_{mn})$$

$$\Phi_{34}\left(\vec{R}_{mn}\right)=\Phi_{43}\left(\vec{R}_{mn}\right)=\left(\frac{l}{4\pi j\omega\mu r_{mn}}\right)\left(\frac{3(1+j\beta r_{mn})-r_{mn}{}^{2}\beta^{2}}{r_{mn}{}^{4}}\right)x_{mn}y_{mn}\exp(-j\beta r_{mn})$$

$$\Lambda_{23}\left(\vec{R}_{mn}\right)=\left(\frac{l}{4\pi j\omega\mu r_{mn}}\right)\left(\frac{3(1+j\beta r_{mn})-r_{mn}{}^{2}\beta^{2}}{r_{mn}{}^{4}}\right)x_{mn}z_{mn}\exp(-j\beta r_{mn})$$

$$\Phi_{44}\left(\vec{R}_{mn}\right)=\left(\frac{l}{4\pi j\omega\mu r_{mn}}\right)\left\{\frac{\left[3x_{mn}^{2}-r_{mn}{}^{2}\right]}{r_{mn}{}^{3}}\left(\frac{1}{r_{mn}}+j\beta\right)+\beta^{2}\left(1-\frac{y_{mn}^{2}}{r_{mn}{}^{2}}\right)\right\}\exp(-j\beta r_{mn})$$

$$\Lambda_{24}\left(\vec{R}_{mn}\right)=\left(\frac{l}{4\pi j\omega\mu r_{mn}}\right)\left(\frac{3(1+j\beta r_{mn})-r_{mn}{}^{2}\beta^{2}}{r_{mn}{}^{4}}\right)y_{mn}z_{mn}\exp(-j\beta r_{mn})$$

Notice that $\Phi_{21}(\vec{R}_{mn})$ contains a factor of $\frac{1}{\varepsilon}$ and $\Phi_{34}(\vec{R}_{mn})$ contains a factor of $\frac{1}{\mu}$.

Thus $\Phi_{21}(\vec{R}_{mn})$ could be written as $\eta_0^2\Phi_{34}(\vec{R}_{mn})$ where η_0 is the intrinsic impedance of free space. Similarly $\Phi_{11}(\vec{R}_{mn}) = \eta_0^2\Phi_{33}(\vec{R}_{mn})$ and $\Phi_{22}(\vec{R}_{mn}) = \eta_0^2\Phi_{44}(\vec{R}_{mn})$ so the matrix $\Phi(\vec{R}_{mn})$ becomes

$$\Phi(\vec{R}_{mn}) = \begin{bmatrix} \eta_0{}^2\Phi_{33}(\vec{R}_{mn}) & \eta_0{}^2\Phi_{34}(\vec{R}_{mn}) & 0 & \Phi_{14}(\vec{R}_{mn}) \\ \eta_0{}^2\Phi_{34}(\vec{R}_{mn}) & \eta_0{}^2\Phi_{44}(\vec{R}_{mn}) & -\Phi_{14}(\vec{R}_{mn}) & 0 \\ 0 & -\Phi_{14}(\vec{R}_{mn}) & \Phi_{33}(\vec{R}_{mn}) & \Phi_{34}(\vec{R}_{mn}) \\ \Phi_{14}(\vec{R}_{mn}) & 0 & \Phi_{34}(\vec{R}_{mn}) & \Phi_{44}(\vec{R}_{mn}) \end{bmatrix} \tag{2.41}$$

Therefore,

$$\Lambda(\vec{R}_{mn}) = \begin{bmatrix} \eta_0{}^2\Phi_{33}(\vec{R}_{mn}) & \eta_0{}^2\Phi_{34}(\vec{R}_{mn}) & 0 & \Phi_{14}(\vec{R}_{mn}) \\ \eta_0{}^2\Phi_{33}(\vec{R}_{mn}) & \eta_0{}^2\Phi_{44}(\vec{R}_{mn}) & -\Phi_{14}(\vec{R}_{mn}) & 0 \\ \Lambda_{11}(\vec{R}_{mn}) & \Lambda_{12}(\vec{R}_{mn}) & -\Lambda_{21}(\vec{R}_{mn}) & -\Lambda_{22}(\vec{R}_{mn}) \\ 0 & -\Phi_{14}(\vec{R}_{mn}) & \Phi_{33}(\vec{R}_{mn}) & \Phi_{34}(\vec{R}_{mn}) \\ \Phi_{14}(\vec{R}_{mn}) & 0 & \Phi_{34}(\vec{R}_{mn}) & \Phi_{34}(\vec{R}_{mn}) \\ \Lambda_{21}(\vec{R}_{mn}) & \Lambda_{22}(\vec{R}_{mn}) & \Lambda_{23}(\vec{R}_{mn}) & \Lambda_{24}(\vec{R}_{mn}) \end{bmatrix} \tag{2.42}$$

2.5. CALCULATE ELECTRIC AND MAGNETIC FIELD USING THE MODEL

Once the values of dipole currents have been found, the electric and magnetic fields at any point in the space would be given by

$$\begin{bmatrix} E_x(\vec{r}_1) \\ E_y(\vec{r}_1) \\ E_z(\vec{r}_1) \\ H_x(\vec{r}_1) \\ H_y(\vec{r}_1) \\ H_z(\vec{r}_1) \\ \vdots \\ E_x(\vec{r}_M) \\ E_y(\vec{r}_M) \\ E_z(\vec{r}_M) \\ H_x(\vec{r}_M) \\ \vec{H}_y(\vec{r}_M) \\ H_z(\vec{r}_M) \end{bmatrix} = \begin{bmatrix} \Lambda(\vec{R}_{11}) & \cdots & \Lambda(\vec{R}_{M1}) \\ \vdots & & \vdots \\ \Lambda(\vec{R}_{1N}) & \cdots & \Lambda(\vec{R}_{MN}) \end{bmatrix} \begin{bmatrix} I_{ex}(\vec{r}_1') \\ I_{ey}(\vec{r}_1') \\ I_{mx}(\vec{r}_1') \\ I_{my}(\vec{r}_1') \\ \vdots \\ I_{ex}(\vec{r}_N') \\ I_{ey}(\vec{r}_N') \\ I_{mx}(\vec{r}_N') \\ I_{my}(\vec{r}_N') \end{bmatrix} \tag{2.43}$$

In the procedure of modeling, the number of dipoles depends on the number of measurement points or the numbers of points we take from simulation. The position of the dipoles also relates to how many points we take from the DUT. For example, the positions are different when we take an array of $[26\times 26]$ dipoles and $[14\times 14]$ dipoles, assuming the two arrays cover the same area. Meanwhile, the dipoles are required to be considered as infinitesimal.

3. VALIDATION OF THE EQUIVALENT DIPOLE SOURCE

3.1. SIMULATION IN HFSS

As shown below, a microstrip hybrid was constructed in HFSS to study the radiation at 2cm from the trace. The purpose of this part is to get all the fields components information needed to build the equivalent source, in Matlab, based on electric and magnetic dipoles.

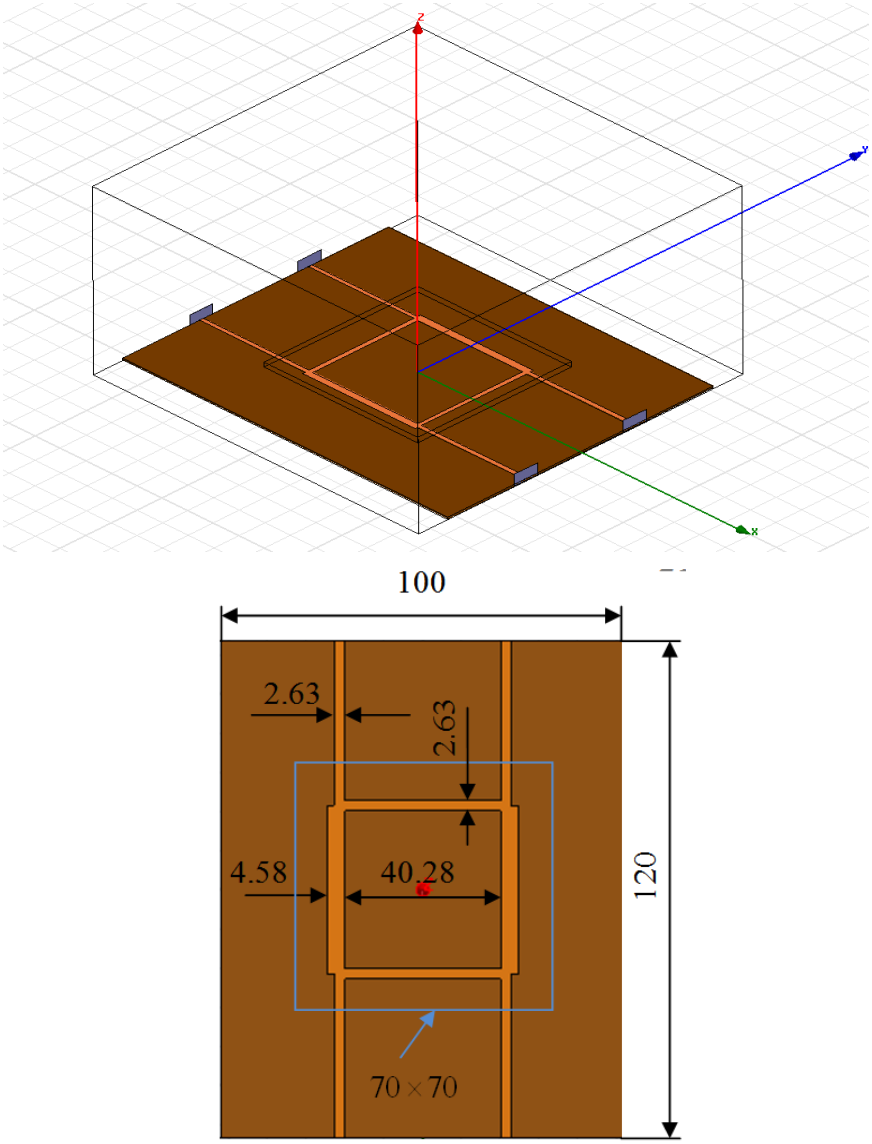

Figure 3.1 Microstrip hybrid model in HFSS (units: mm)

The hybrid is excited with wave ports at a single frequency 960MHz. The source power is set to be one watt. The sizes of the traces are determined in EZpp to make sure the hybrid has an input impedance of 50 Ω. There is an air box above the trace, which is used to study electromagnetic fields above the trace. The dimensions of that air box are $70mm \times 70mm \times 3mm$. The lower face of the box is 2mm from the trace. Boundary conditions are applied to the trace and the ground plane. Both of them are PEC. The biggest box holding the whole structure is an air box set for radiation boundary conditions.

Results from the simulation are shown as below:

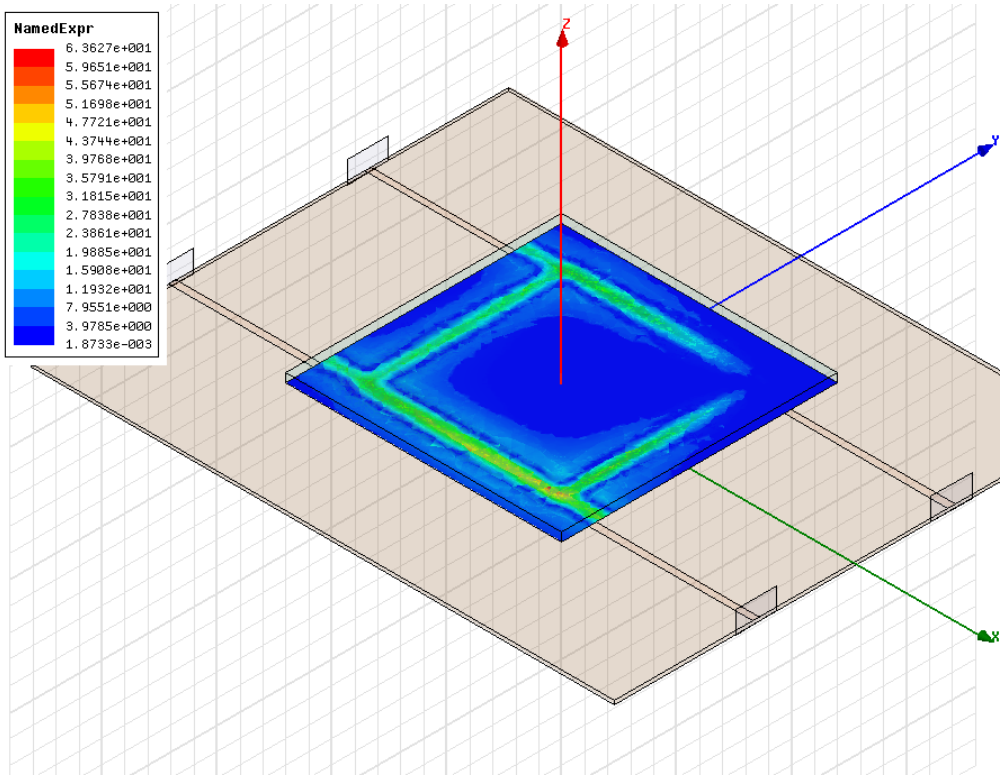

Figure 3.2 $|Hz|$ simulated at 2mm above the trace using HFSS (units: A/m)

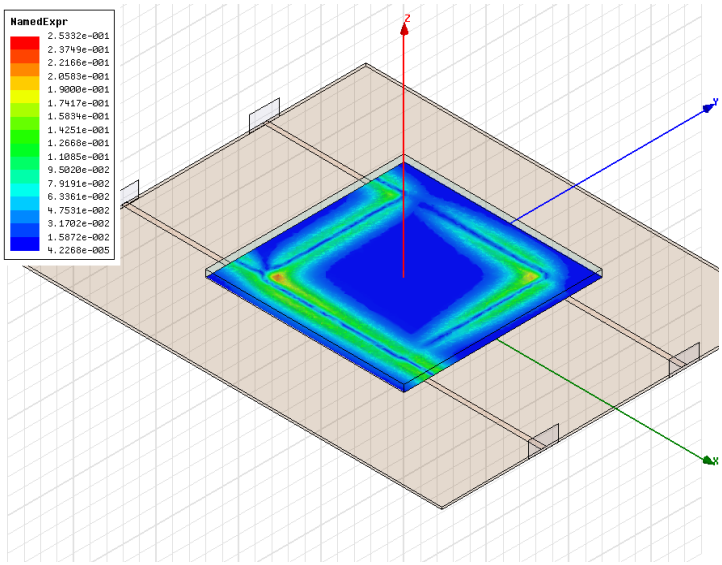

Figure 3.3 $|Ez|$ simulated at 2mm above the trace using HFSS (units: V/m)

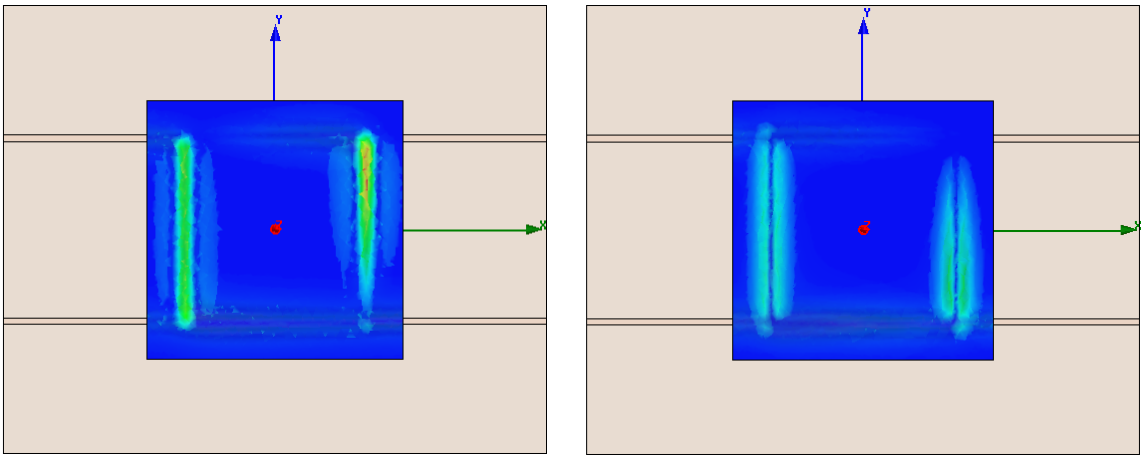

Figure 3.4 $|Hx|$ (left, Units: A/m), $|Ex|$ (right, Units: V/m) simulated at 2mm above the trace using HFSS

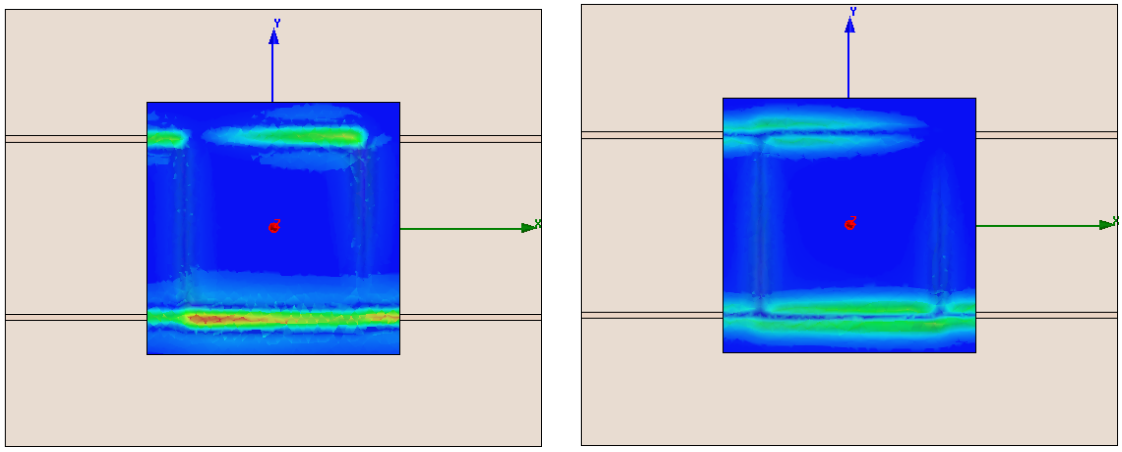

Figure 3.5 $|Hy|$(left, Units: A/m), $|Ey|$(right, Units: V/m) simulated at 2 mm above the trace using HFSS

H and E field data are saved in a file to be imported in Matlab. In this case, x and y component of both H and E field are used to build the equivalent model source.

3.2. DERIVE EQUIVALENT DIPOLE MODEL SOURCE IN MATLAB

Once we get all the information from HFSS simulation, the crossed dipole model is ready to predict electric and magnetic fields at a certain distance from the source. This equivalent source model built, in Matlab, is made up of an array of 26×26 crossed dipole sets. Each dipole set contains 2 electric dipoles and 2 magnetic dipoles. The length of each dipole is 1mm. It's considered to be electrically small at 960 MHz in free space.

In this part, the crossed dipole model source will be compared to the tilted dipole model developed in ESIGELEC [1], [2].

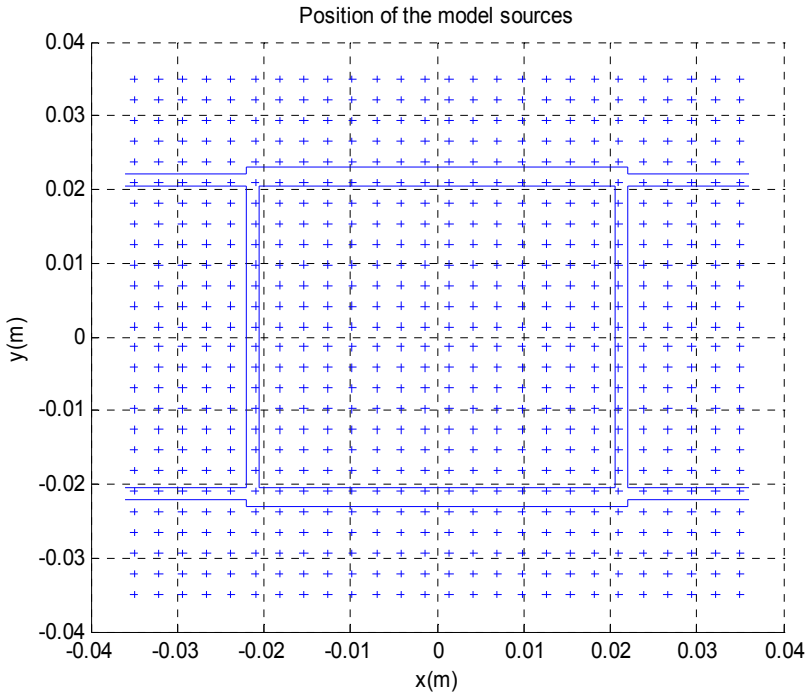

Figure 3.6 Position and orientation of the crossed dipoles

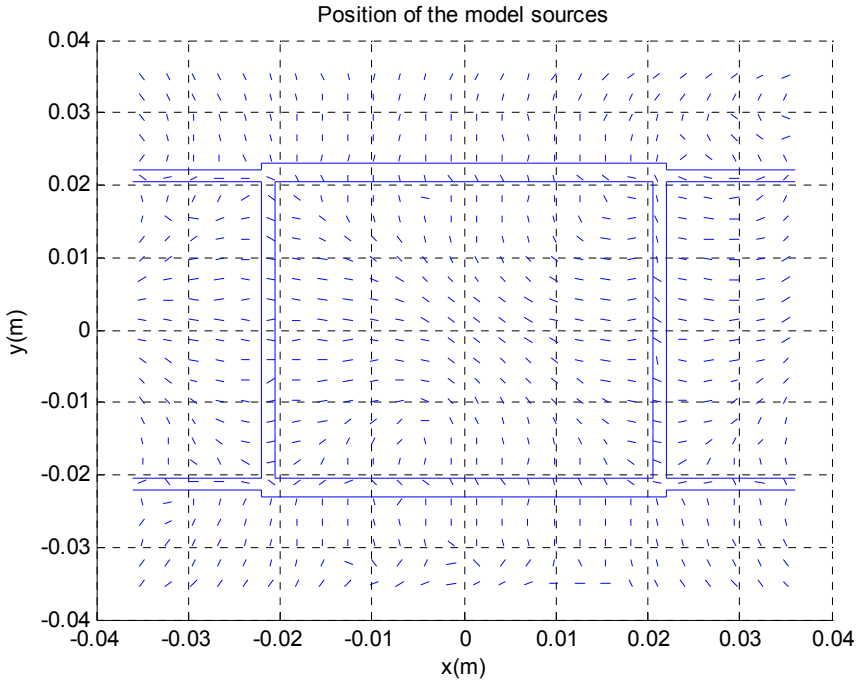

Figure 3.7 Position and orientation of the tilted dipoles

The dipoles are on the same plane as the trace. The number of the dipoles is determined by the length of the dipole and the dimension of the device under test (microstrip hybrid in this case). It is important to ensure the dipoles do not overlap one another, and to use as many dipoles as possible to get an accurate model. Then the number of dipoles will be decreased to see how well the model works with fewer dipoles. In this case, 1352 electric dipoles and1352 magnetic dipoles work well. Results are shown in the next section and they will be compared to the fields predicted by tilted dipole model source.

3.3. COMPARING RESULTS FROM HFSS AND THE EQUIVALENT SOURCE MODEL

The electromagnetic fields generated by the equivalent source model are simulated in Matlab for both the crossed dipole and tilted dipole models. Electric and magnetic fields are calculated at 2mm and 5mm above the source plane. Results are shown as below. Figure 3.8 and Figure 3.10 show the magnitude of the individual electric and/or magnetic field components using the crossed dipole model, using a commercial full wave simulation program (HFSS), and using the tilted dipole model. Figure 3.9 and Figure 3.11 show the phase of the individual electric and/or magnetic field components using the crossed dipole model, using a commercial full wave simulation program (HFSS), and using the tilted dipole model.

In order to quantity the differences represented in these figures, the relative error at each dipole location was computed using the following formula:

$$error_{local}(x,y) = \frac{\left|Field_{HFSS}(x,y) - Field_{Matlab}(x,y)\right|}{\left|Field_{HFSS}(x,y)\right|}$$

Since the field at some points may be very small comparing to the field right above the trances, the relative error calculated at those locations may be extremely large.

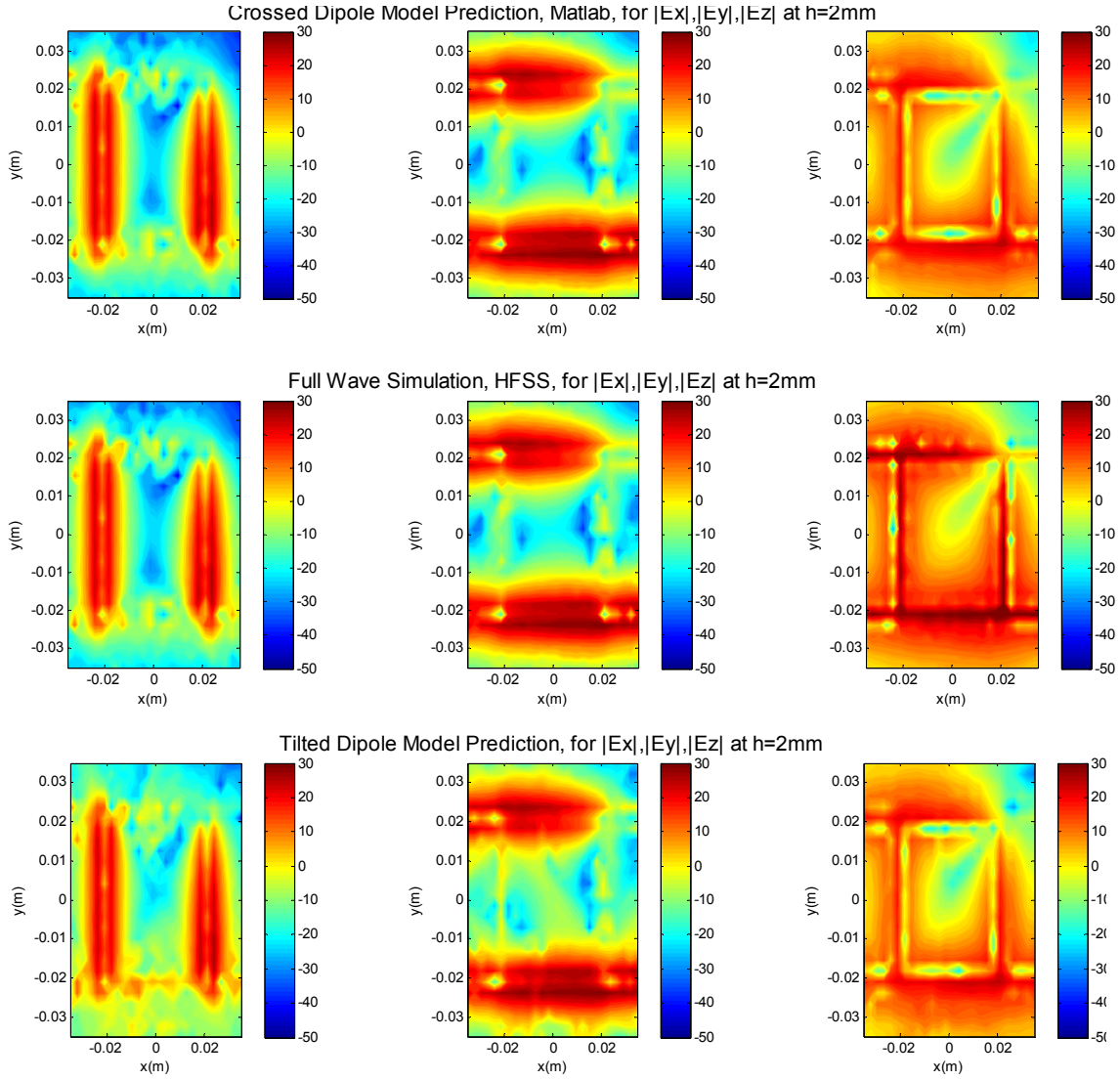

Figure 3.8 Magnitude of E field predicted by the crossed dipole source, HFSS and tilted dipole source at h=2mm (Units: dBV/m)

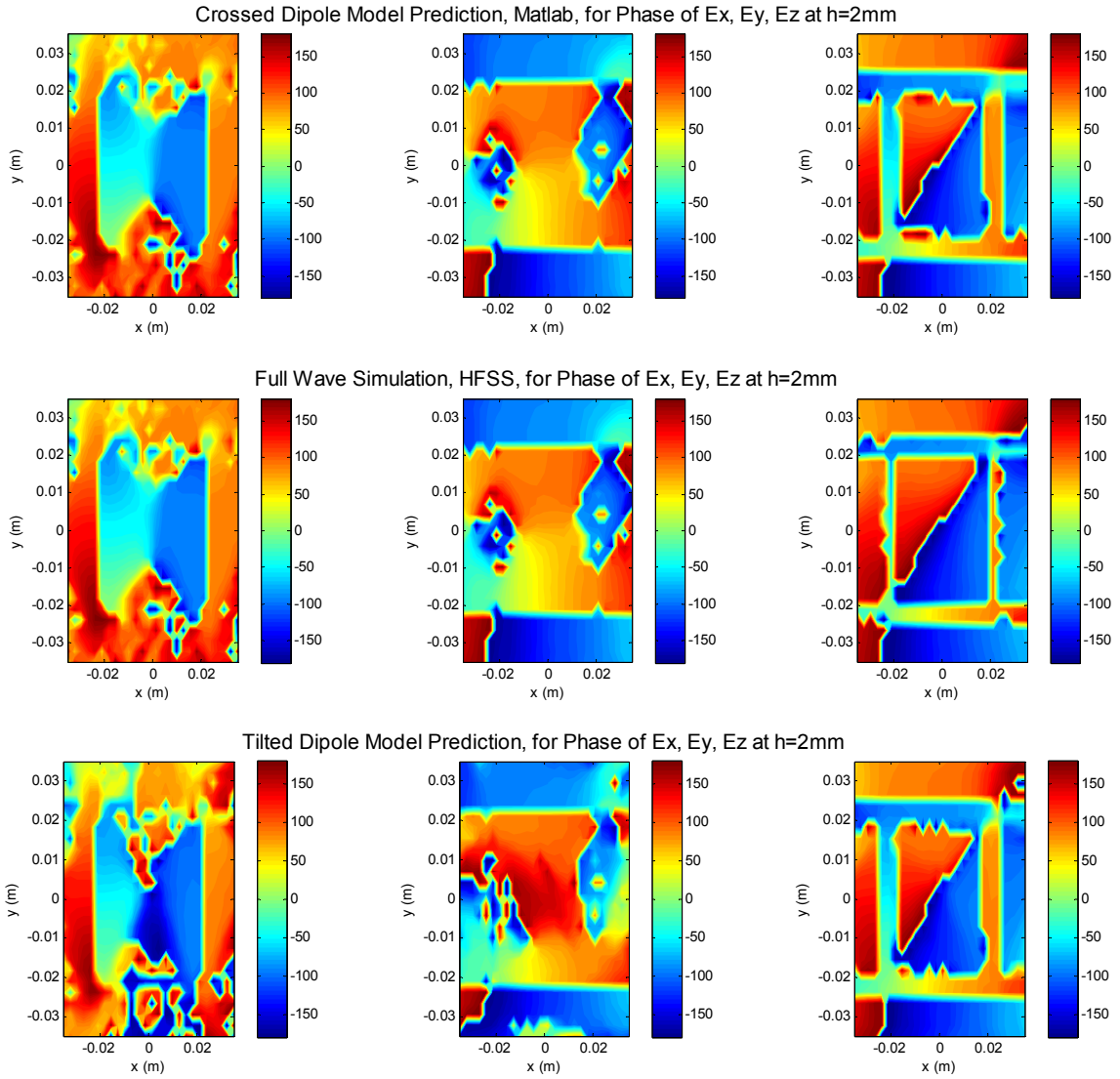

Figure 3.9 Phase of E field predicted by the crossed dipole source, HFSS and tilted dipole source at h=2mm (Units: deg)

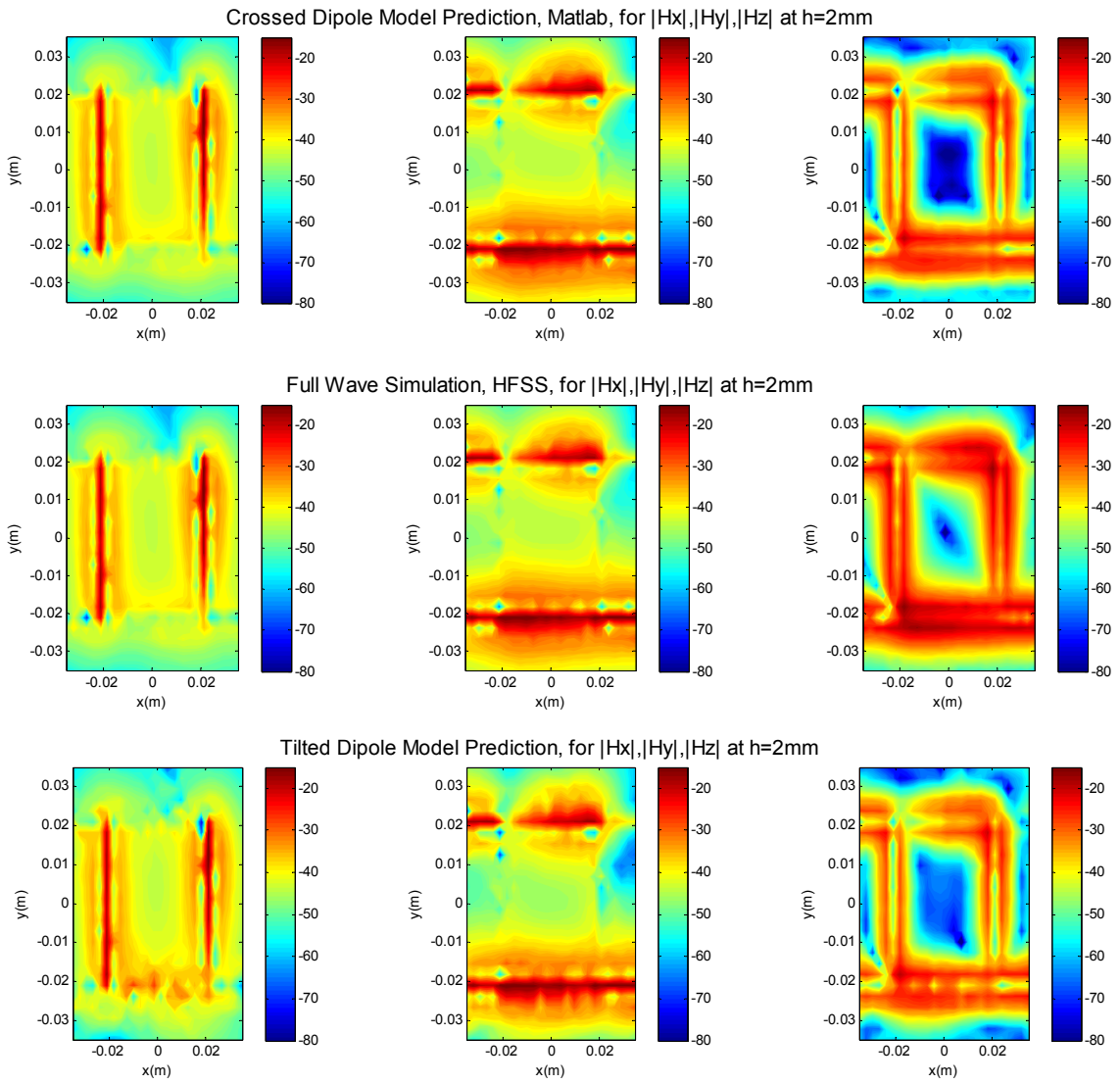

Figure 3.10 Magnitude of H field predicted by the crossed dipole source, HFSS and tilted dipole source at h=2mm (Units: dBA/m)

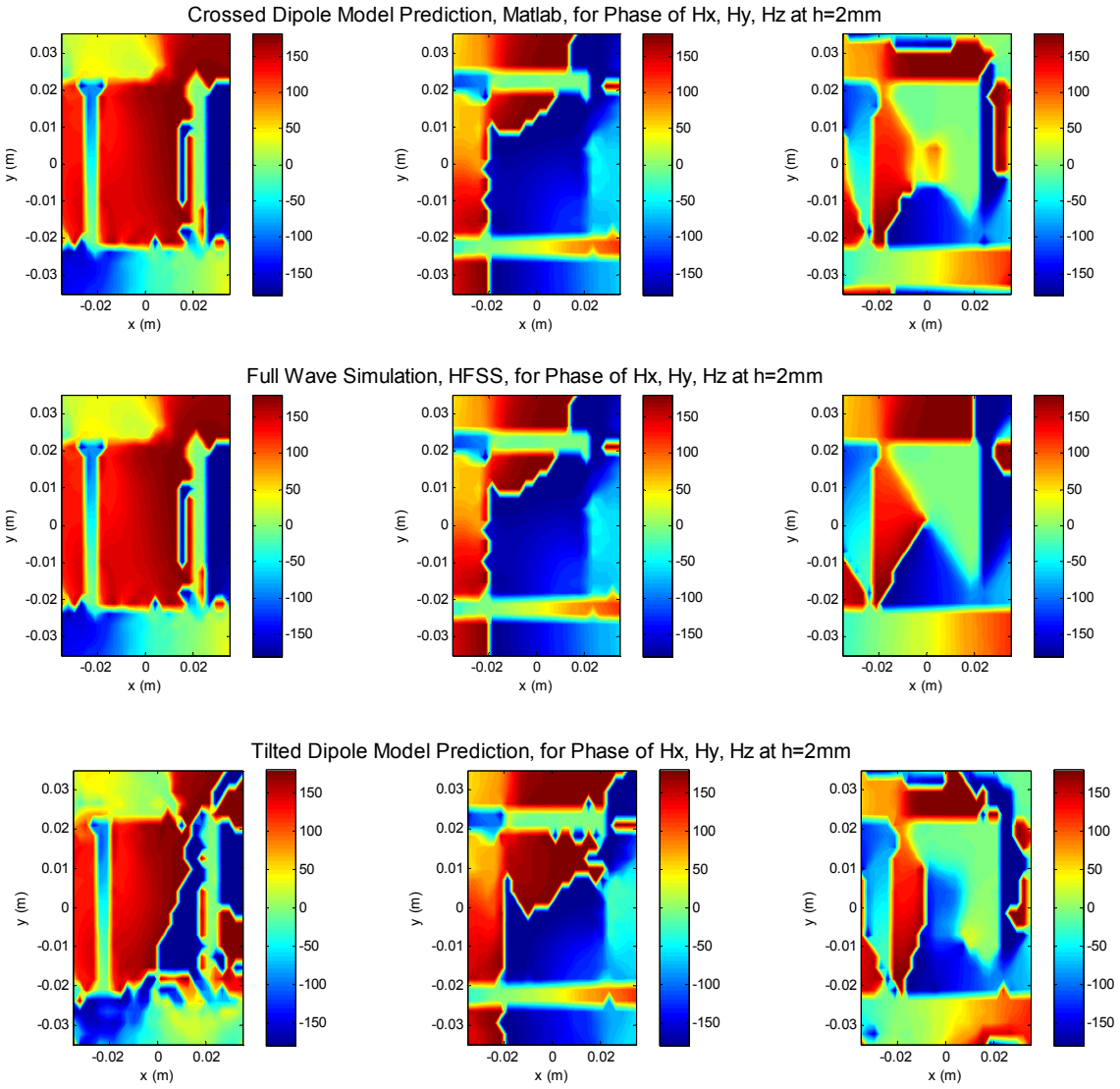

Figure 3.11 Phase of H field predicted by the crossed dipole source, HFSS and tilted dipole source at h=2mm (Units: deg)

For this reason, the weighted error is used to evaluate the accuracy of the dipole model. The weighted error was computed using the following formula:

$$error_{weighted}(x,y) = \frac{error_{local}(x,y) \times \left| Field_{HFSS}(x,y) \right|}{\max \left| TotalField_{HFSS}(x,y) \right|} = \frac{error_{local}(x,y)}{\max \left| TotalField_{HFSS}(x,y) \right|}$$

$$\left| TotalField_{HFSS}(x,y) \right| = \sqrt{\left| Field_{x\_HFSS}(x,y) \right|^2 + \left| Field_{y\_HFSS}(x,y) \right|^2 + \left| Field_{z\_HFSS}(x,y) \right|^2}$$

$Field_{HFSS}(x,y)$ represents any one field component as simulated in HFSS.

$Field_{Matlab}(x,y)$ represents the same field component as calculated in Matlab for the equivalent dipole model. The mean error is defined as the value of the weighted error averaged over all values of x and y in the images presented above.

$$mean\ weighted\ error = \frac{\sum_{x=1,y=1}^{x,y} error_{weighted}(x,y)}{xy} \times 100\%$$

For crossed dipole model:

$$\left| E_x \right|_{mean\ weighted\ error} = 4.3108 \times 10^{-15}\% \quad \left| H_x \right|_{mean\ weighted\ error} = 7.7673 \times 10^{-15}\%$$

$$\left| E_y \right|_{mean\ weighted\ error} = 6.4705 \times 10^{-14}\% \quad \left| H_y \right|_{mean\ weighted\ error} = 1.3794 \times 10^{-14}\%$$

$$\left| E_z \right|_{mean\ weighted\ error} = 5.11\% \qquad \left| H_z \right|_{mean\ weighted\ error} = 5.76\%$$

Errors from the tilted dipole model are:

$$\left| E_x \right|_{mean\ weighted\ error} = 0.73\% \quad \left| H_x \right|_{mean\ weighted\ error} = 0.86\%$$

$$\left| E_y \right|_{mean\ weighted\ error} = 0.79\% \quad \left| H_y \right|_{mean\ weighted\ error} = 0.99\%$$

$$\left| E_z \right|_{mean\ weighted\ error} = 11.35\% \quad \left| H_z \right|_{mean\ weighted\ error} = 5.34\%$$

In this case both models (the tilted dipole model and the crossed dipole model) seem to yield fairly accurate results. However, the crossed dipole model will allow the x and y components of the source currents for each dipole to be modeled independently in both magnitude and phase. This would seem to be advantageous in modeling fields with elliptical or circular polarization. In addition the relationship between the dipole currents in the equivalent crossed dipole source model and the field components on a given plane can be expressed in terms of linear equations while the relationship between

the dipole current and orientation angle in the tilted dipole model may require a nonlinear relationship. In comparing the execution times for finding the crossed dipole model and the tilted dipole model it appears that the crossed dipole model runs faster, at least for the code implementation used in this thesis.

A further measure of the usefulness of the equivalent dipole source models is the ability of the models to predict the electromagnetic fields on a second horizontal plane parallel to the measurement plane but located at some distance above the measurement plane. The next set of figures shows the fields predicted at 5 mm above the plane containing the traces of the hybrid. Figure 3.12 and Figure 3.14 show the magnitude of the individual electric and/or magnetic field components using the crossed dipole model, using a commercial full wave simulation program (HFSS), and using the tilted dipole model. Figure 3.13 and Figure 3.15 show the phase of the individual electric and/or magnetic field components using the crossed dipole model, using a commercial full wave simulation program (HFSS), and using the tilted dipole model.

Mean weighted errors are calculated again in this case. The results are show below:

Errors from the crossed dipole model:

$$|E_x|_{mean\ weighted\ error} = 3.92\% \quad |H_x|_{mean\ weighted\ error} = 4.34\%$$
$$|E_y|_{mean\ weighted\ error} = 6.51\% \quad |H_y|_{mean\ weighted\ error} = 7.05\%$$
$$|E_z|_{mean\ weighted\ error} = 5.03\% \quad |H_z|_{mean\ weighted\ error} = 9.00\%$$

Errors from the tilted dipole model:

$$|E_x|_{mean\ weighted\ error} = 3.97\% \quad |H_x|_{mean\ weighted\ error} = 4.11\%$$
$$|E_y|_{mean\ weighted\ error} = 7.88\% \quad |H_y|_{mean\ weighted\ error} = 5.18\%$$
$$|E_z|_{mean\ weighted\ error} = 8.85\% \quad |H_z|_{mean\ weighted\ error} = 10.28\%$$

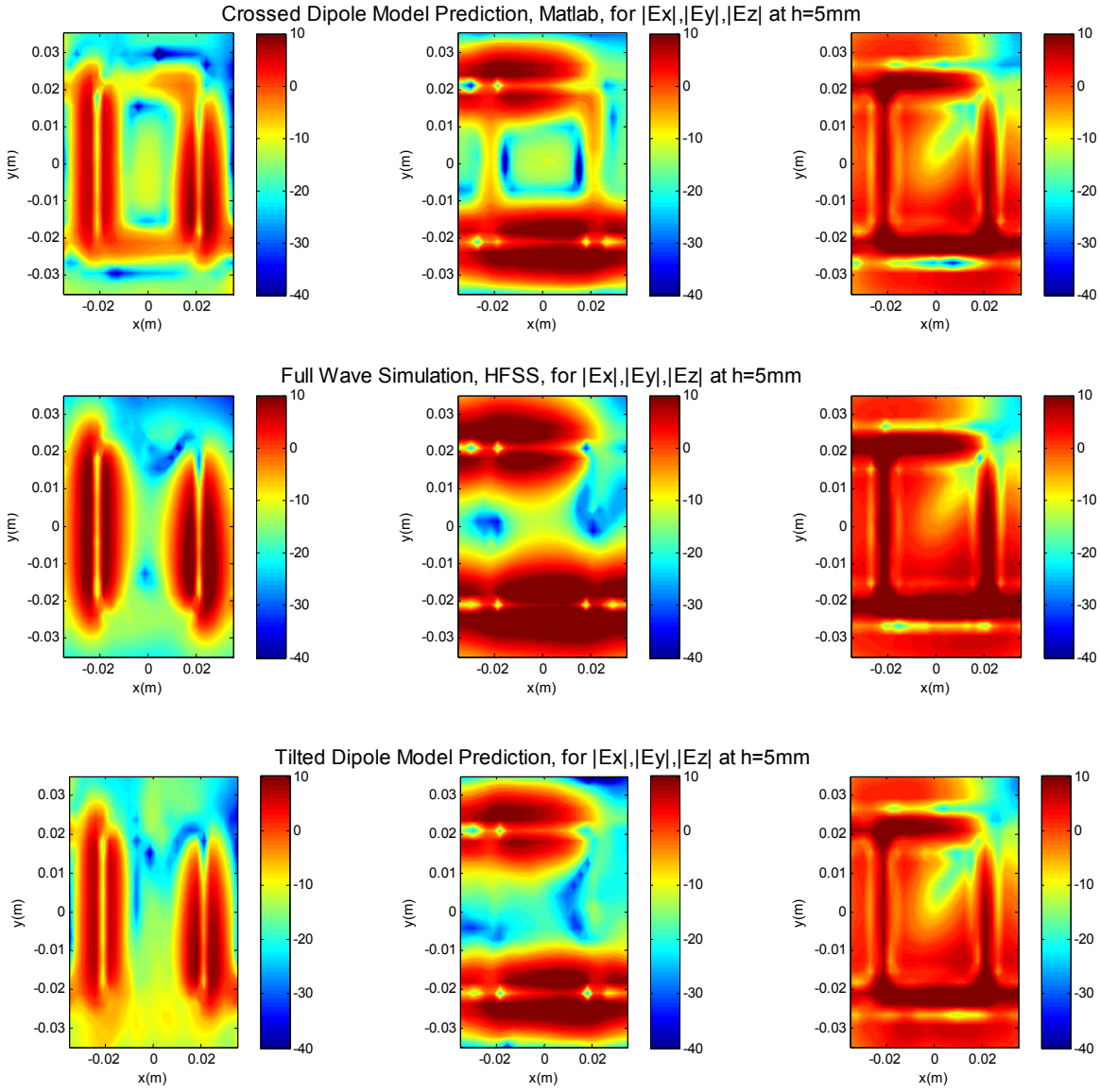

Figure 3.12 Magnitude of E field predicted by the crossed dipole source, HFSS and tilted dipole source at h=5mm (Units: dBV/m)

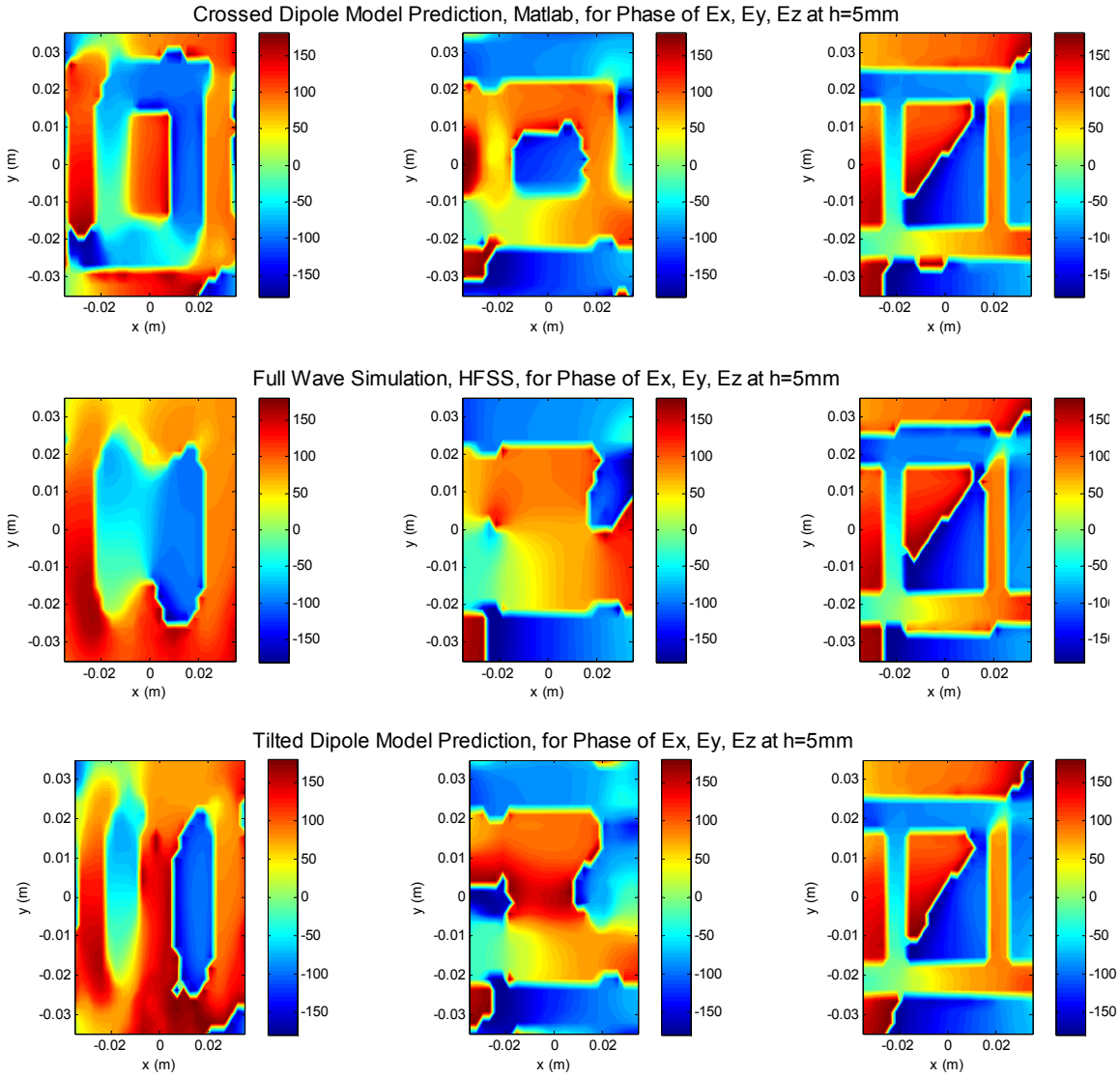

Figure 3.13 Phase of E field predicted by the crossed dipole source, HFSS and tilted dipole source at h=5mm (Units: deg)

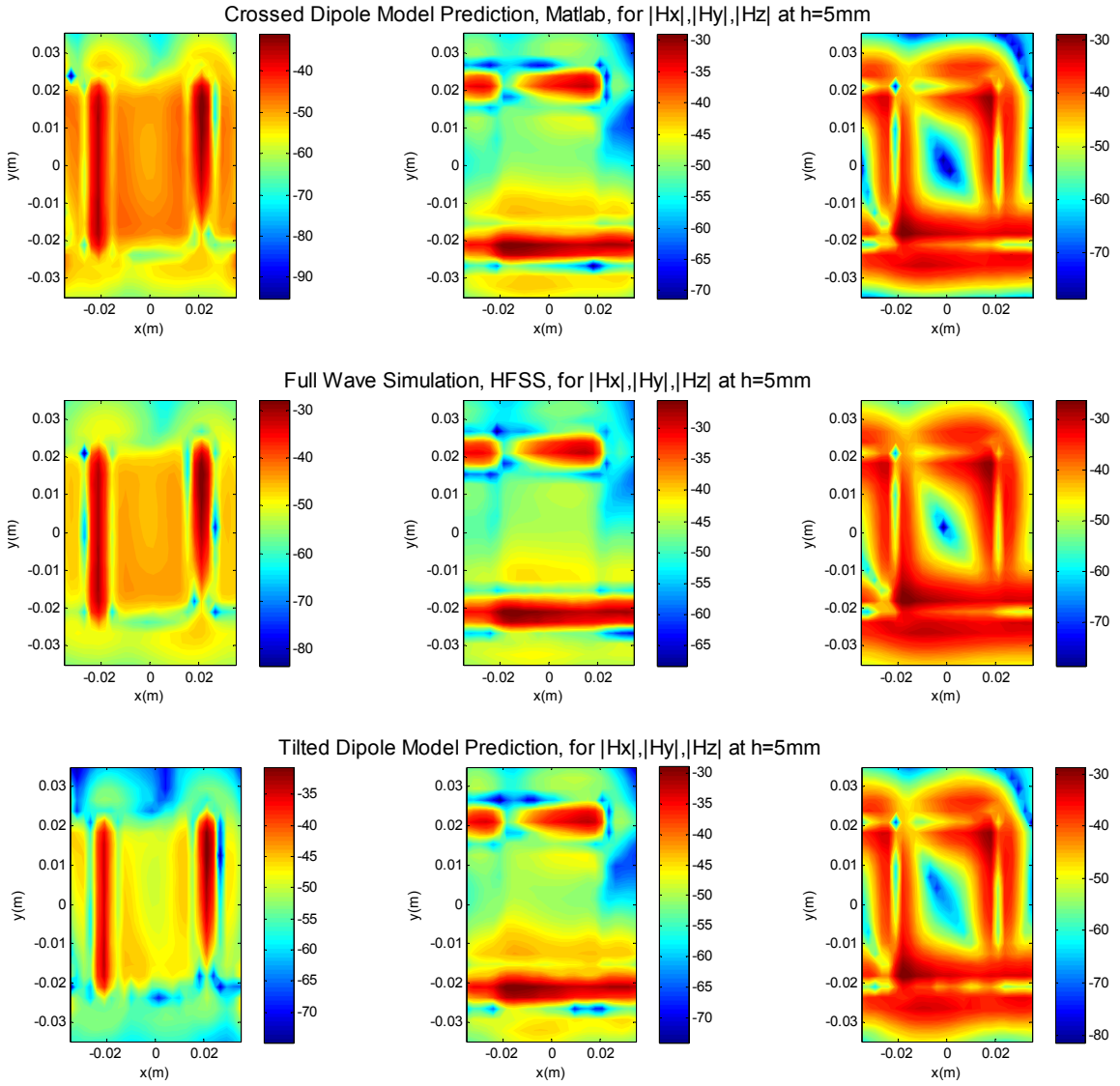

Figure 3.14 Magnitude of H field predicted by the crossed dipole source, HFSS and tilted dipole source at h=5mm (Units: dBA/m)

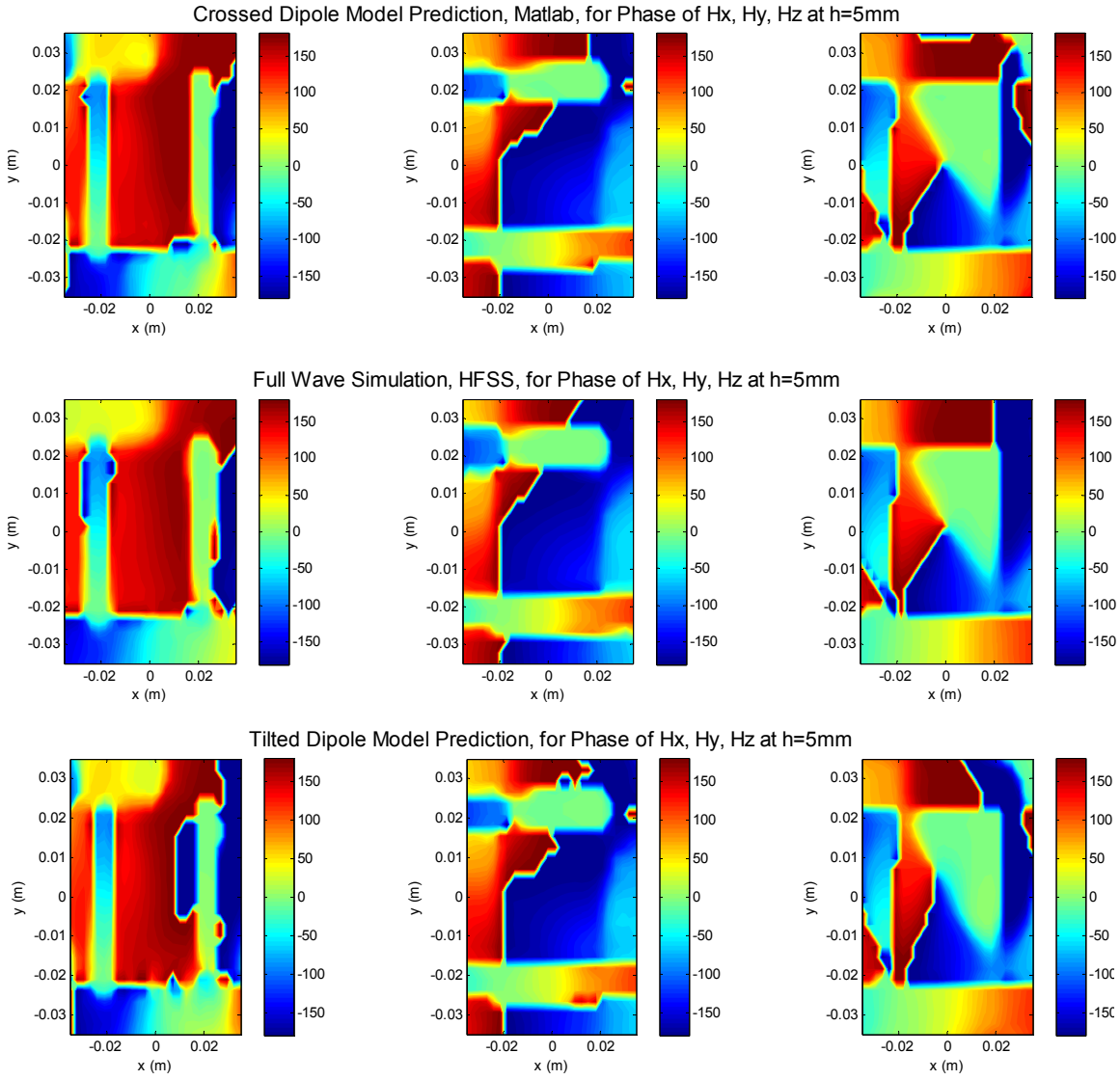

Figure 3.15 Phase of H field predicted by the crossed dipole source, HFSS and tilted dipole source at h=5mm (Units: deg)

From this set of comparisions, 4 of the 6 field components predicted by the crossed dipole source model are more accurate than the field prediction from the tilted dipole model. The errors are all below 9%. Since the equivalent dipole source is obtained by potential functions, it is able to calculate electric and magnetic fields at any distance from the source. In this case, near field data are used to construct the model. It may also enable the model to predict far field radiation based on this information. However, this part is not verified in this thesis.

4. APPLICATION OF NEAR-FIELD SCANNING MEASUREMENT

Near-field scanning measurement is a practical way to verify the methodology presented above. While full wave simulation is an easy way to construct the model, it's always better to see how this method could be applied to the "real world". To get the field information, either Vector Network Analyzer or Spectrum Analyzer could be used. However, the experiment setup is relatively complicated for a spectrum analyzer to get the phase of the electric and magnetic fields. [1] In this case, a Vector Network Analyzer is used to measure S21 and the phase of the fields ($H_{x,}\ H_{y,}\ E_{x,}\ E_{y,}$).

4.1. MAGNETIC FIELD MEASUREMENT

The Near-Field Scanning system (Smart Scan) used in this experiment is developed in MST EMCLab. The test bench is constituted by a 3 axes robot, which enables the system to measure x, y, and z components of the fields. A 5 by 5 square magnetic probe is place 2mm (and 5mm) over the microstrip hybrid. The normal direction of the loop is either perpendicular or orthogonal to x axis or y axis depends on with field component we are taking. The hybrid is made exactly of the same size as the one built in HFSS. It has four ports. One of them is connected to VNA port1. The source power is set to be 10dBmW. The other three ports of the hybrid are terminated with 50 ohm loads. During the experiment, fields are taken in an area of $70mm \times 70mm$ 2mm above the traces and 5mm above the traces, which is also the same as in the simulation procedure. Port 2 of VNA is connected to the probe. Frequency is centered at 960MHz with a span of 20MHz. S21 and phase information is written in a file during the experiment for future use. The configuration of the experiment is presented as below in Figure 4.1.

The magnetic probe (black holder PCB probe as shown in Figure 4.2) is also designed in MST EMCLab. The coupling measurement of H field shows that the probe is good up to 1GHz (shown in Figure 4.3). [7]

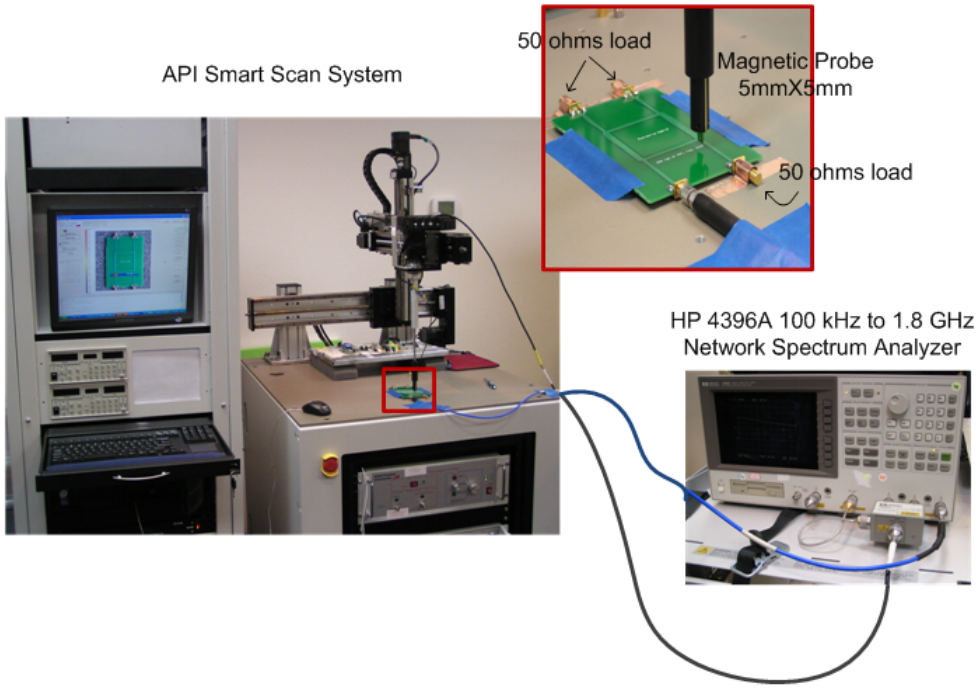

Figure 4.1 Setup of near-field scanning

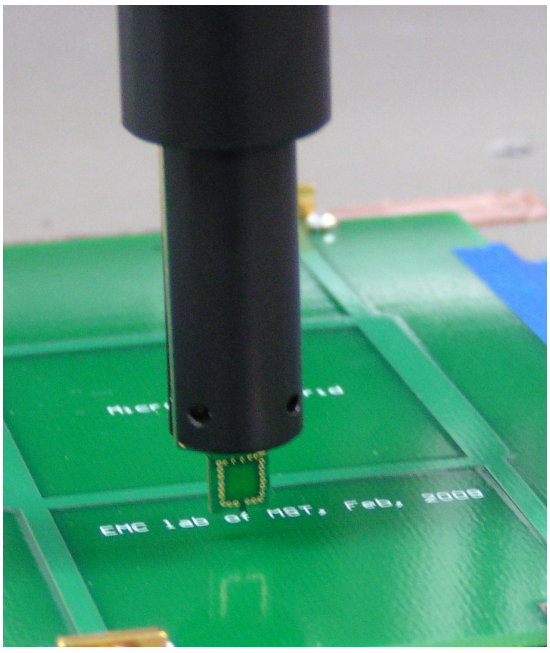

Figure 4.2 H field probe with a $5mm \times 5mm$ square loop

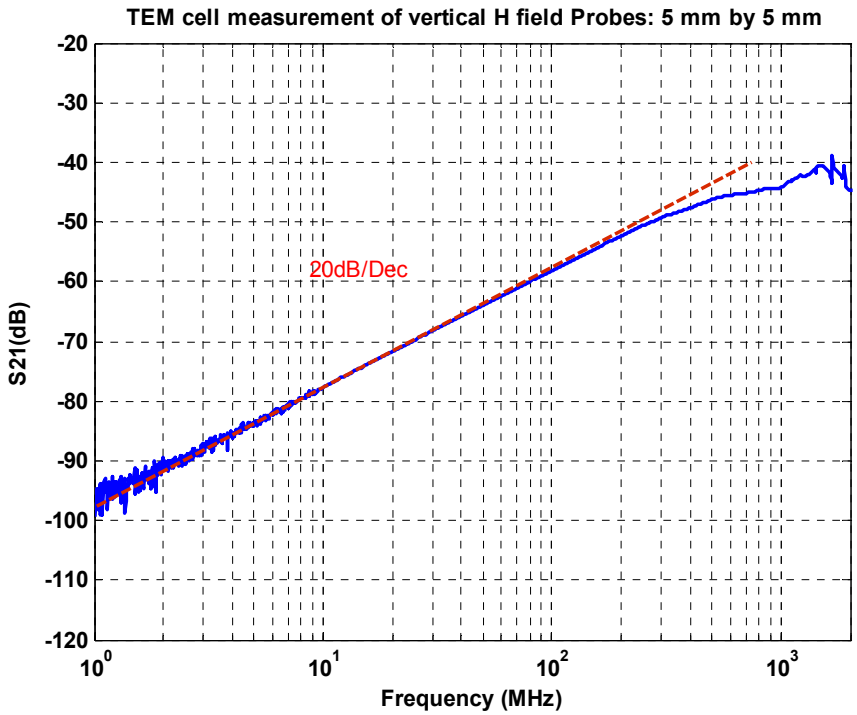

Figure 4.3 TEM Cell measurement of the magnetic probe

Before the test is run, the number of the measurement points is determined according to the size of the microstrip hybrid and the length of each dipole. In this case, to be consistent with full wave simulation, a 26×26 array is arranged in the centered area with a size of $70mm \times 70mm$.

Here are results from near-field scanning measurements drawn by the scanning system.

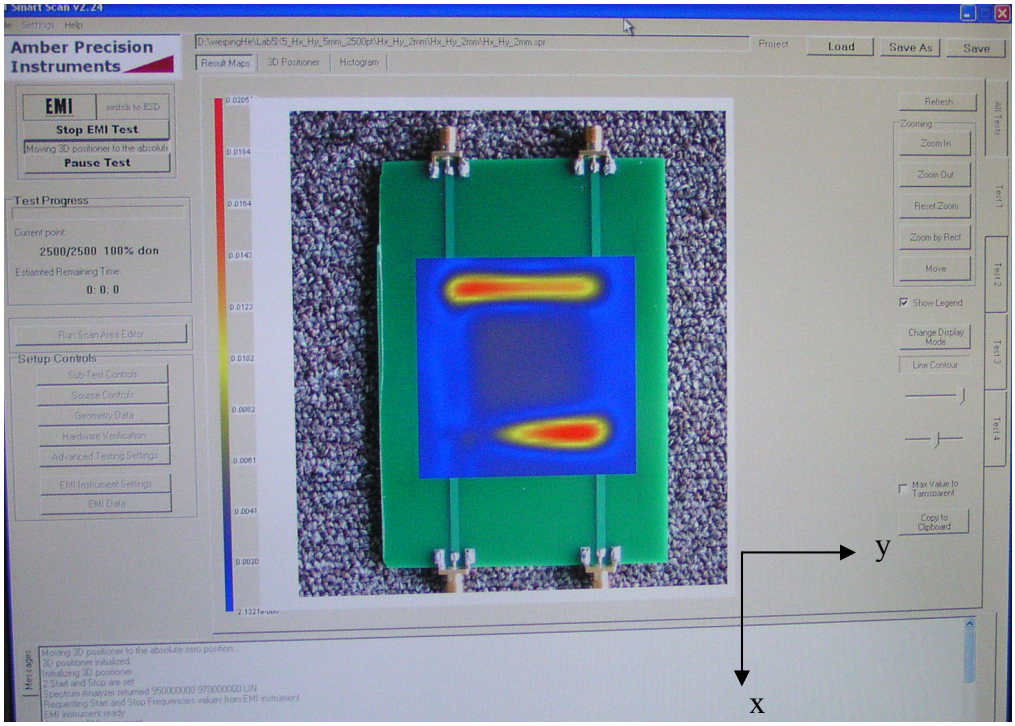

Figure 4.4 Hx from near-field scanning at h=2mm

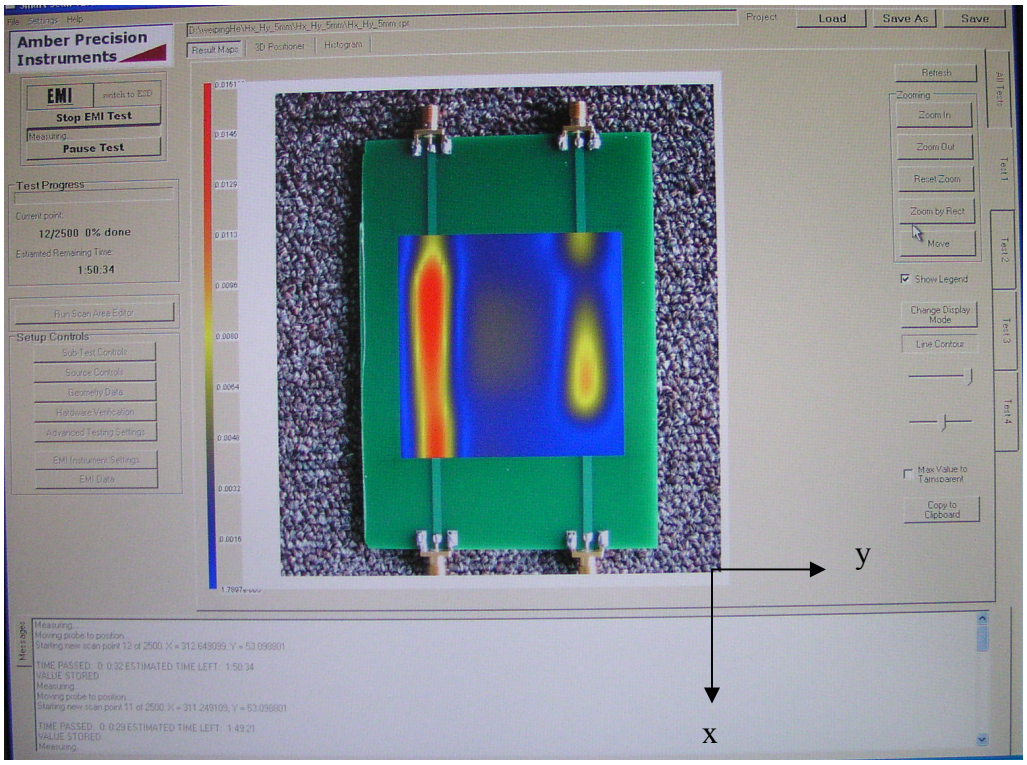

Figure 4.5 Hy from near-field scanning at h=2mm

4.2. ELECTRIC FIELD MEASUREMENT

The setup of the electric field measurement is basically same as shown in figure 4.1 except that a hybrid should be added to the differential electric field probe before it's connected to port 2 of the VNA. Other settings are the same as in the magnetic field measurement.

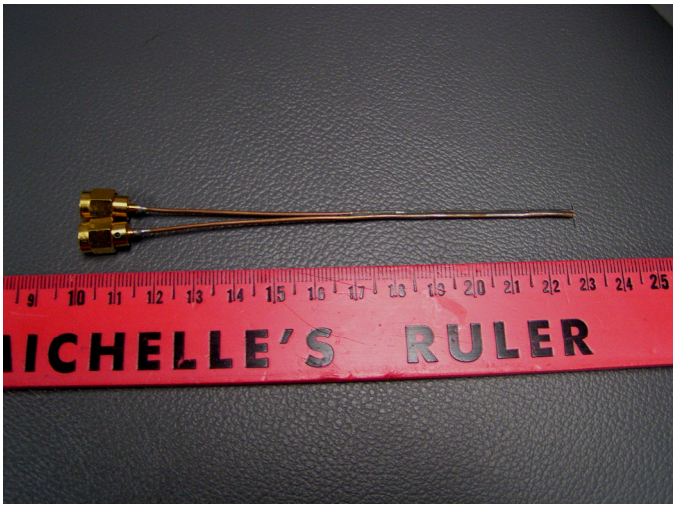

Figure 4.6 Differential electric field probe

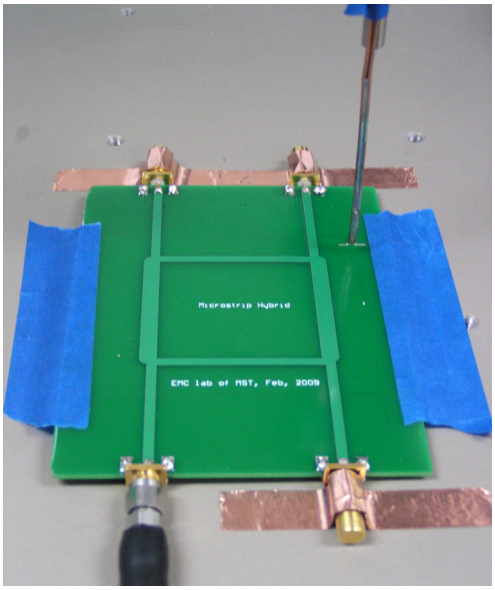

Figure 4.7 Differential electric field probe in use

E field scanning results are shown as below:

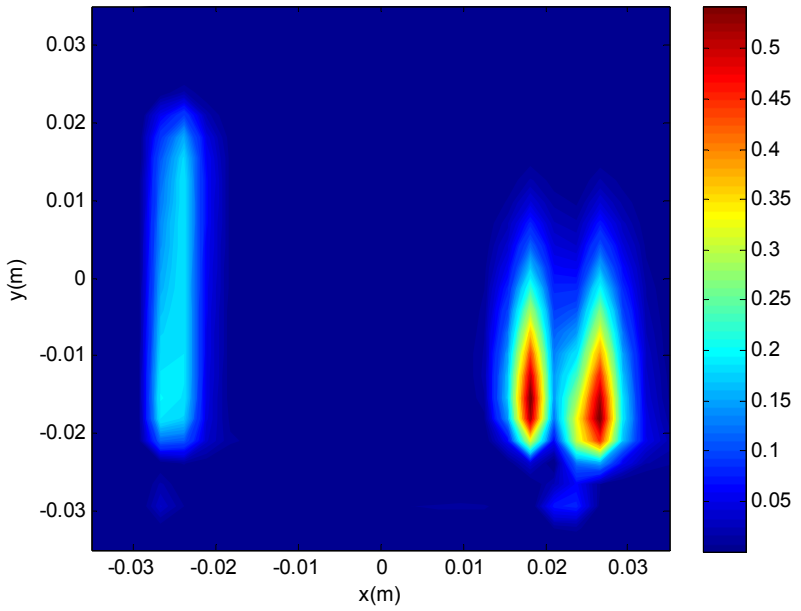

Figure 4.8 Ex from near-field scanning at h=2mm (Units: V/m)

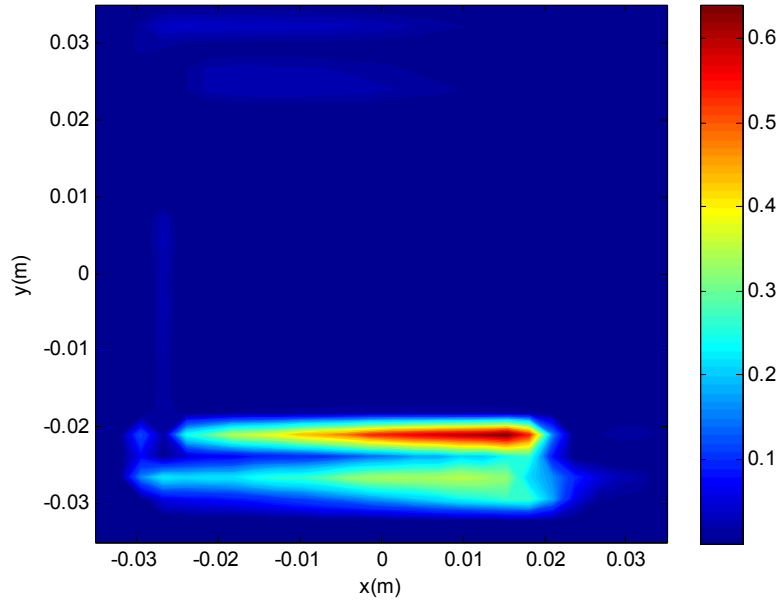

Figure 4.9 Ey from near-field scanning at h=2mm (Units: V/m)

4.3. COMPARE RESULTS FROM NEAR-FIELD SCANNING AND THE EQUIVALENT MODEL

Now the information collected from the experiment (E_x, E_y, H_x, H_y at 2mm) serves as the input of the model. Equivalent sources are obtained by the fields measured at 2mm. Again results are compared at 5mm to verify the accuracy of the equivalent source. Figure 4.10 and Figure 4.12 show the magnitude and phase of the electric field components using the crossed dipole model and from near-field scanning. Figure 4.11 and Figure 4.13 show the magnitude and phase of the magnetic field components using the crossed dipole model and from near-field scanning.

From the field plots and the error calculation, the results at 5mm are not as good as expected. The phase discrepancy is obvious, especially for H_y . These disturbances might be due to the following reasons:

When making measurements at 2mm, there is a good chance to have the distance shorter or longer than 2mm, which is not a problem in HFSS. The equivalent model source is sensitive to this small error. The phase of the fields could be very different even when the distance changes a little. Also, after measuring E_x , the probe turns 90 degrees to measure E_y , the distance between the probe and the source plane will also be slightly changed. All of these could affect the accuracy of the crossed dipole source model.

Phase measured by the network analyzer are not the designed phase of E and H field. The phase measured by the network analyzer is the phase of S_{21} . The probe factor also has a phase associated with it. But this phase information was not taken into account since the model is working at a single frequency 960 MHz. This might cause errors that are larger than expected.

All experiments have random errors. No measurement can be made with infinite precision. To avoid random errors, multiple measurements are required. But data from measurement is an input of the equivalent model source. It is not the focus of this thesis but serves as an indication of how the crossed dipole source model could be used with near-field scanning measurements. For this reason, the experiment was not repeated and it might not show the best result one could get from near-field scanning.

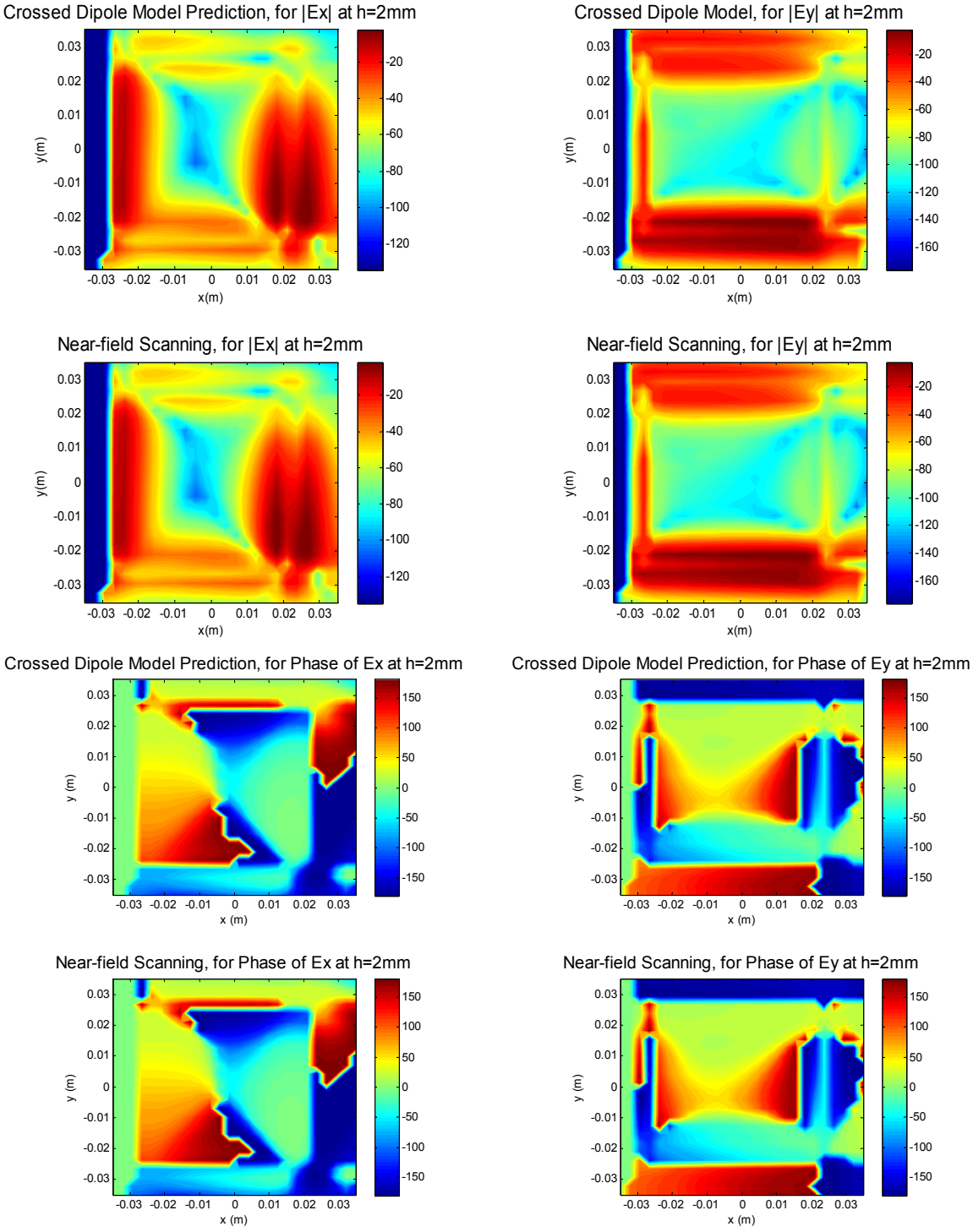

Figure 4.10 E field predicted by the equivalent source and near-field scanning at h=2mm (Units: dBV/m, deg)

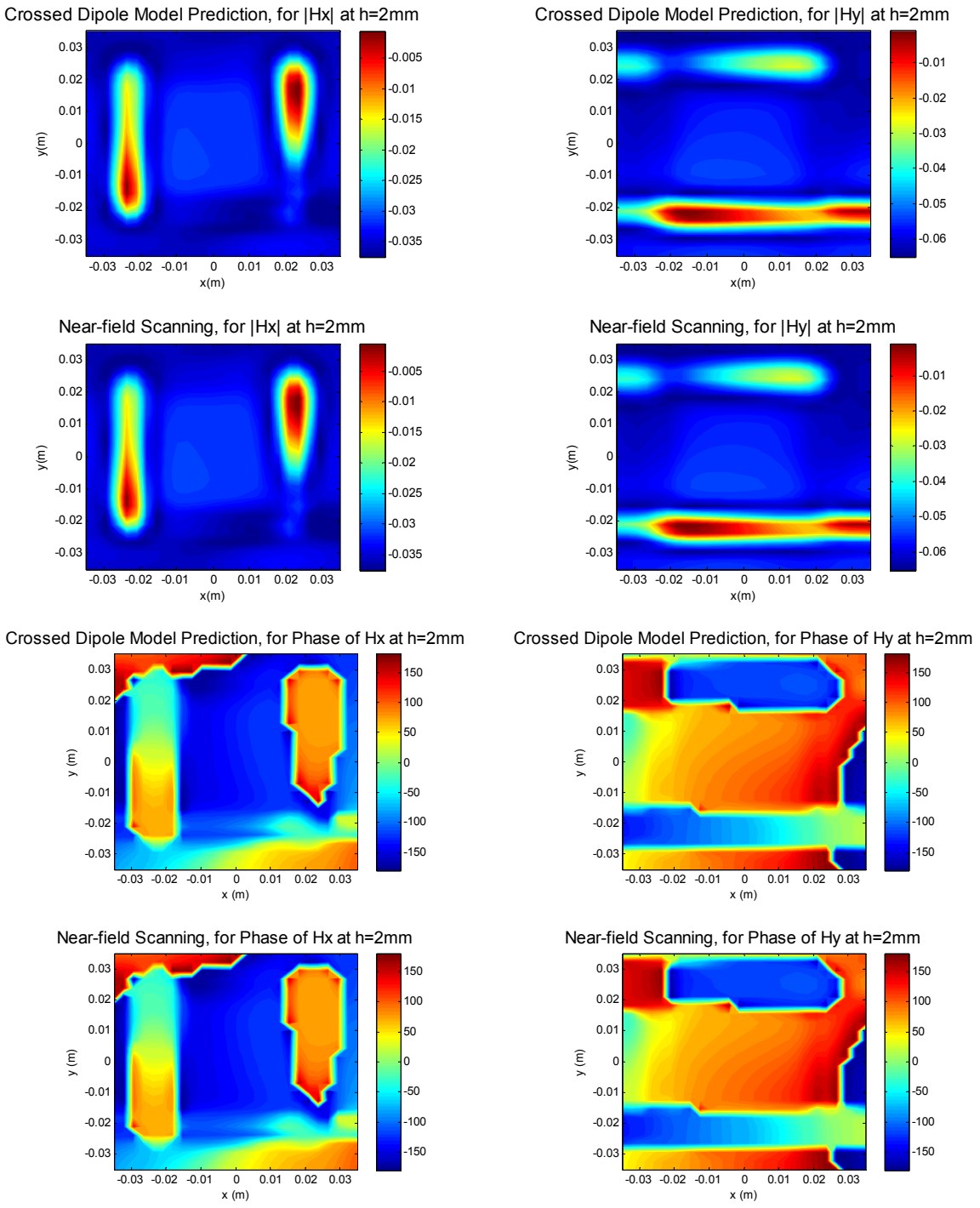

Figure 4.11 H field predicted by the equivalent source and near-field scanning at h=2mm (Units: dBV/m, deg)

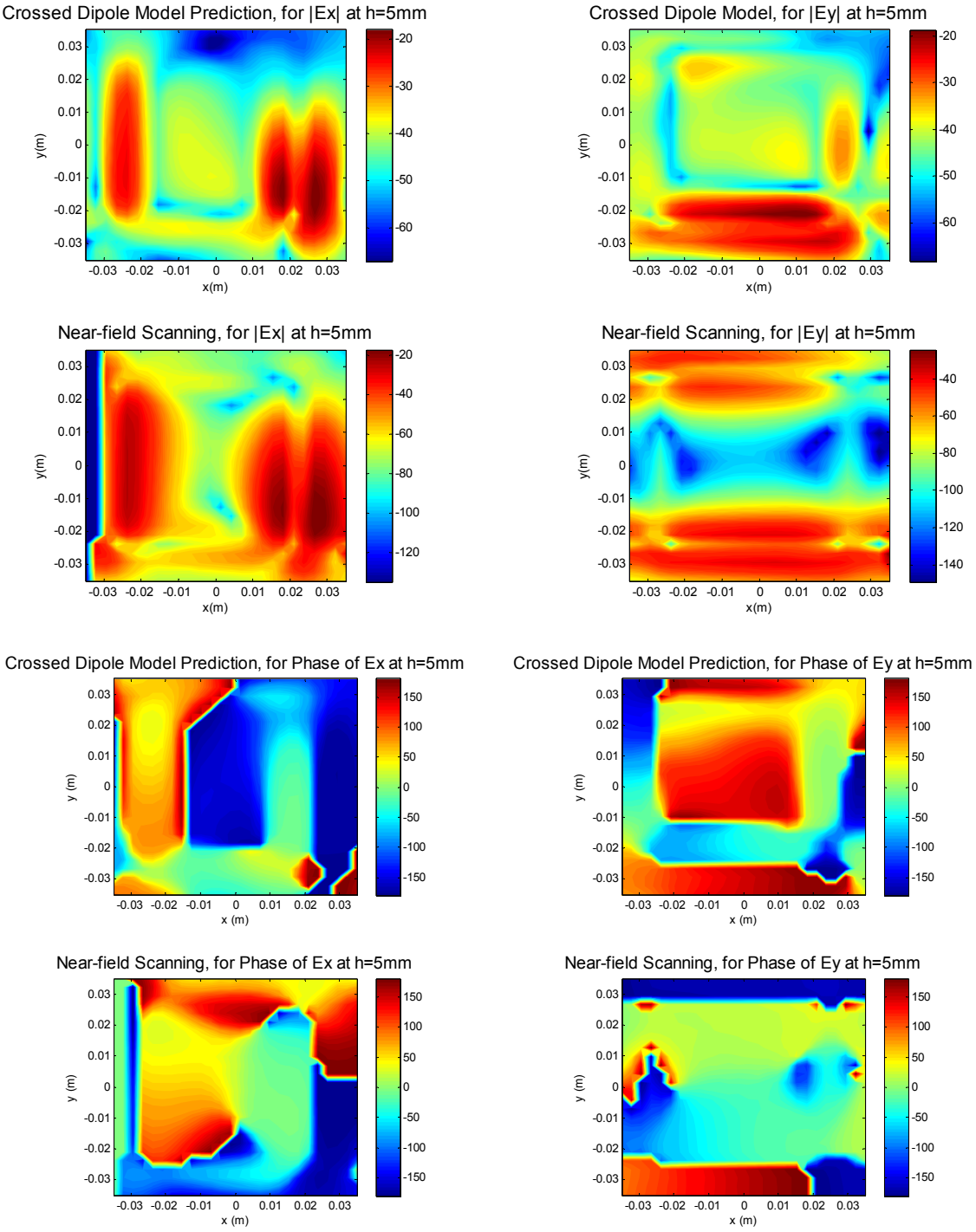

Figure 4.12 E field predicted by the equivalent source and near-field scanning at h=5mm (Units: dBV/m, deg)

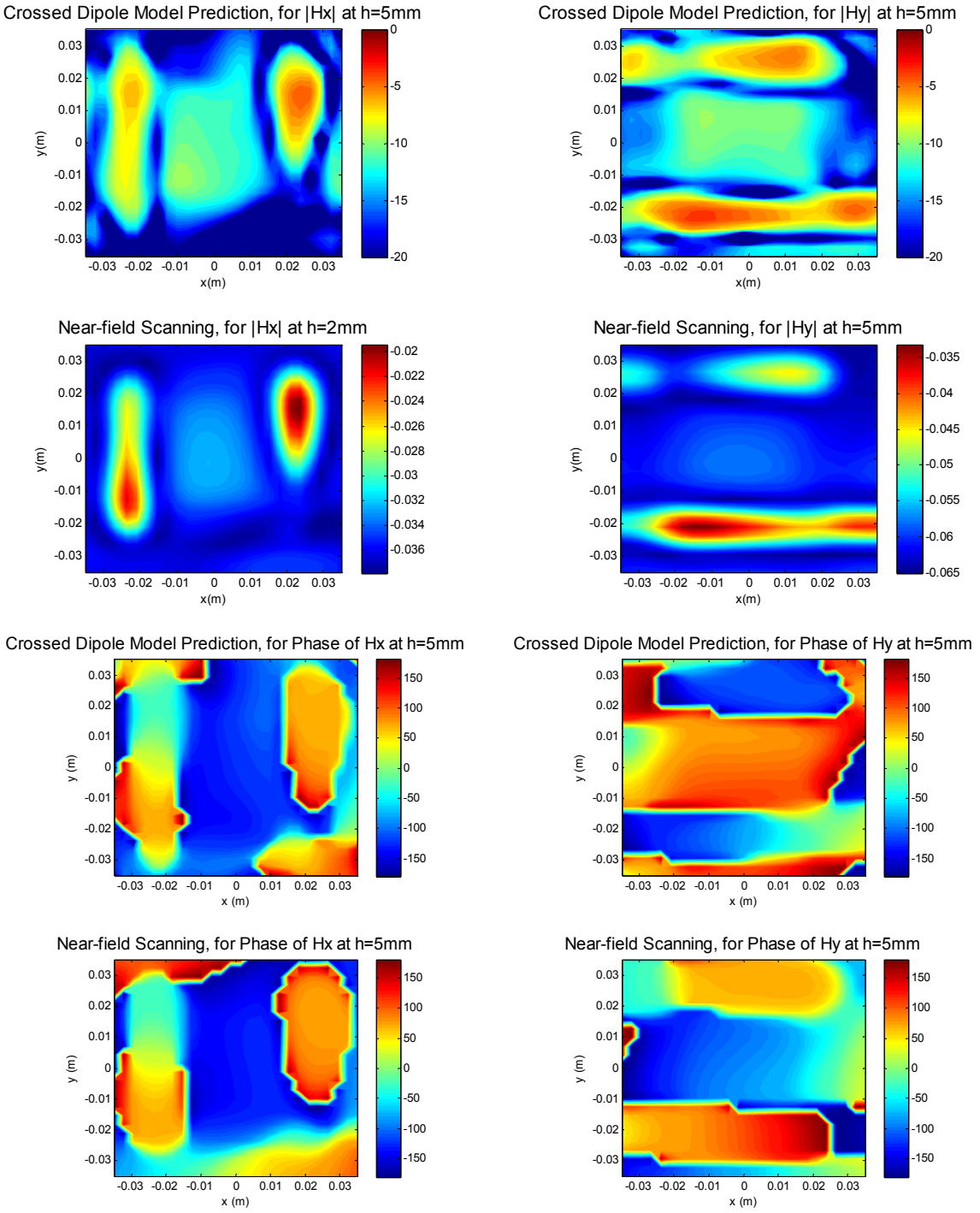

Figure 4.13 H field predicted by the equivalent source and near-field scanning at h=5mm (Units: dBV/m, deg)

5. CONCLUSIONS

The equivalent model based on a set of crossed electric and magnetic dipoles is able to provide an accurate representation of the device under test when characterizing near-field board radiation emissions. The methodology has been verified by HFSS simulation as well as near-field scanning measurements. The details of the techniques developed in this thesis were demonstrated through application to a microstrip hybrid. By extracting $E_{x,}\ E_{y,}\ H_{x,}\ H_{y}$ at a certain distance (2mm above the hybrid) using HFSS or near-field scanning, fields at a variety of distances could be calculated by the model in Matlab. Comparing results from HFSS simulation and the equivalent model, the errors are all within 5%. While the errors from near-field scanning measurements are relatively large, it does not affect the accuracy of the methodology.

In this thesis, both electric and magnetic dipoles are used to obtain the equivalence. Since the orientations of the electric and magnetic dipoles are fixed, the only parameters that need to be solved in the modeling process are the electric and magnetic currents. It involves one matrix inversion in the program, which helps improve both accuracy and running speed of the equivalent model developed in ESIGELEC.

This equivalent model is built on a plane for the reason that circuit components or PCB could be regarded as a plane. It should be interesting to build a 3D model to represent for sources in space in the future. It's expected to be more accurate and it could be used in more cases.

It's also interesting to know whether far field radiation emissions could be predicted from near field scan data using this model. Theoretically far field could be extracted from near field measurement. But it is not easy to do the near field measurement accurately enough to estimate the far field because much of the propagating wave is buried in the evanescent waves and noise in the near field. This could be an important step to try in the future.

APPENDIX

This is an indication of how to get all the parameters when the dipoles are moved from the origin to any point in the plane and how the total fields (e.g. H field) were counted.

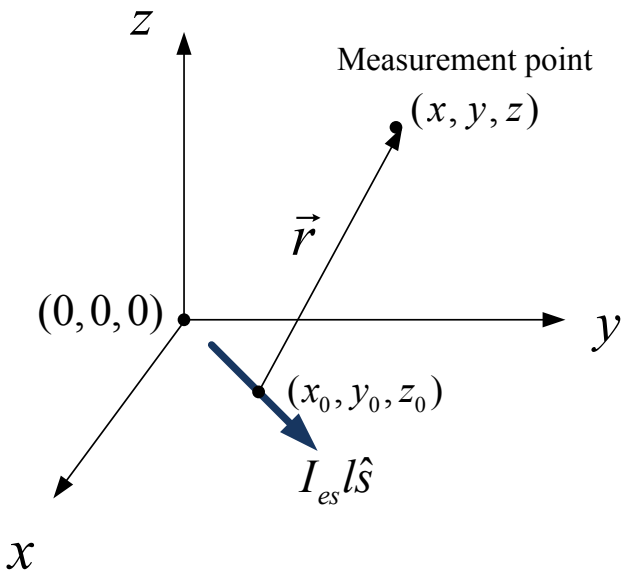

Now move the electric dipole source from origin to any point (x_0, y_0, z_0) in the xy plane, r is the distance between the observation point and the source point. x, y, z is the coordinate of the observation point. Parameters will be changed into:

$$\alpha_{HAx\_y} = (\frac{1}{r^2} + \frac{j\beta}{r})(\frac{l}{4\pi r} e^{-j\beta r})(z - z_0)$$

$$\alpha_{HAy\_y} = 0$$

$$\alpha_{HAz\_y} -(\frac{1}{r^2} + \frac{j\beta}{r})(\frac{I_{ey} l}{4\pi r} e^{-j\beta r})(x - x_0)$$

Where

$$r = \sqrt{(x-x_0)^2 + (y-y_0)^2 + (z-z_0)^2}$$

For a set of horizontal electric dipoles located at $\vec{r}_n$ ' in xy plane having a length of l (which is determined by the frequency of interest to make the dipole infinitesimal), where $n = 1...N$, corresponding current $I_{es1}, I_{es2}, ..., I_{esN}$, total $\vec{H}_A$ at one measurement point

$\vec{r}_1$ is the submission of $\vec{H}_{An}$ from all the dipoles. (Note that total $\vec{H}_A$ is not the total H field measured at a measurement point since we have to take H field from the magnetic dipoles ($\vec{H}_F$) into account.) (x, y, z) is the coordinates of measurement points and (x_0, y_0, z_0) is the center point of the sources (dipoles) as shown below:

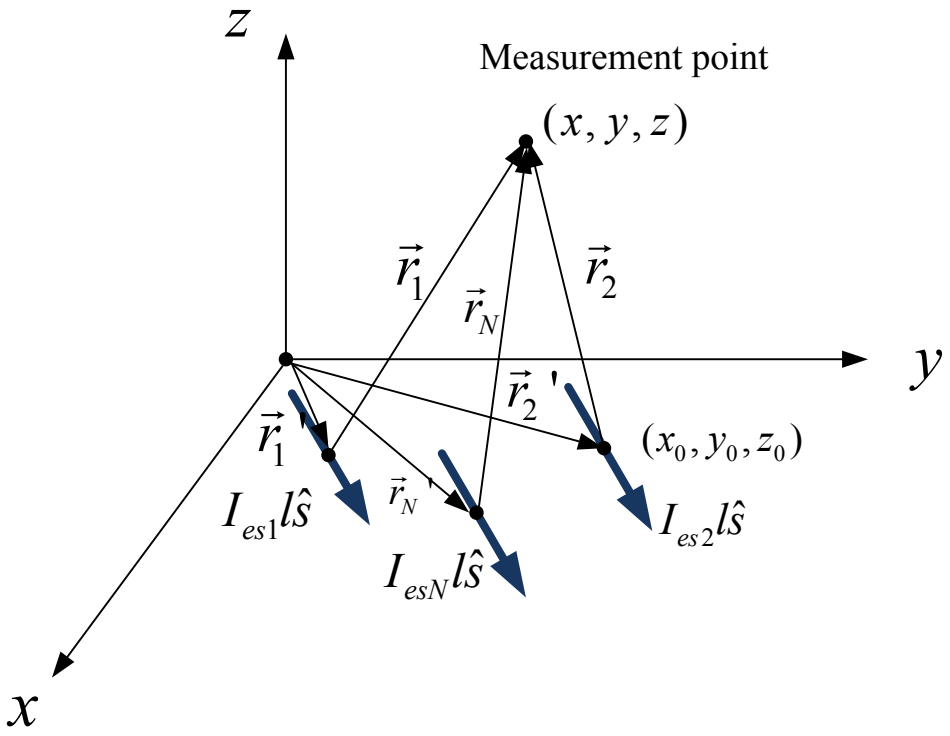

$$H_{Ax}(\vec{r}_1) = \left[\alpha_{HAx\_x1}, \alpha_{HAx\_x2}, \ldots, \alpha_{HAx\_xN}\right] \begin{bmatrix} I_{ex}(\vec{r}_1\,') \\ I_{ex}(\vec{r}_2\,') \\ \vdots \\ I_{ex}(\vec{r}_N\,') \end{bmatrix}$$

$$H_{Ay}(\vec{r}_1) = \left[\alpha_{HAy\_y1}, \alpha_{HAy\_y2}, \ldots, \alpha_{HAy\_yN}\right] \begin{bmatrix} I_{ey}(\vec{r}_1\,') \\ I_{ey}(\vec{r}_2\,') \\ \vdots \\ I_{ey}(\vec{r}_N\,') \end{bmatrix}$$

For a given set of measurement points, $\vec{r}_m$ where $m = 1...M$ and a given set of electric dipoles located at $\vec{r}_n$ where $n = 1...N$, the magnetic field components are the

superposition of all field component also related to current of the electric dipoles through sets of linear equations.

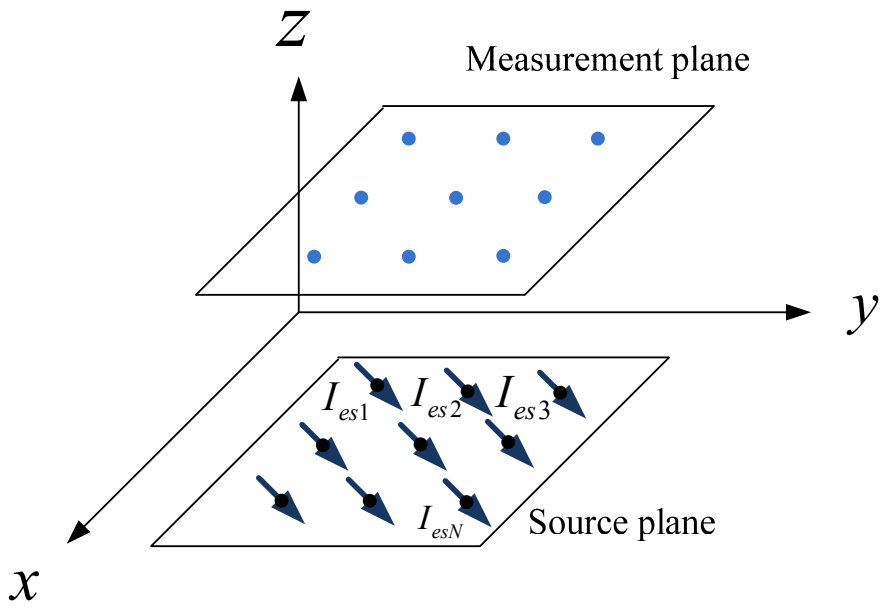

For example the x component of the magnetic field may be written in the form

$$\begin{bmatrix} H_{Ax}(\vec{r}_1) \\ H_{Ax}(\vec{r}_2) \\ : \\ H_{Ax}(\vec{r}_M) \end{bmatrix} = \begin{bmatrix} (\alpha_{HAx})_{11} & (\alpha_{HAx})_{12} & .. & (\alpha_{HAx})_{1N} \\ (\alpha_{HAx})_{21} & .. & .. & (\alpha_{HAx})_{2N} \\ : & : & : & : \\ (\alpha_{HAx})_{M1} & .. & .. & (\alpha_{HAx})_{MN} \end{bmatrix} \begin{bmatrix} I_{ex}(\vec{r}_1\,') \\ I_{ex}(\vec{r}_2\,') \\ : \\ I_{ex}(\vec{r}_N\,') \end{bmatrix}$$

Or more concisely as

$$\left[H_{Ax}(\vec{r}_m)\right]_{m\times 1} = \left[\alpha_{HAx}\right]_{m\times n}\left[I_{ex}(\vec{r}_n\,')\right]_{n\times 1}$$

For y component of the magnetic field:

$$\begin{bmatrix} H_{Ay}(\vec{r}_1) \\ H_{Ay}(\vec{r}_2) \\ \vdots \\ H_{Ay}(\vec{r}_M) \end{bmatrix} = \begin{bmatrix} (\alpha_{HAy})_{11} & (\alpha_{HAy})_{12} & .. & (\alpha_{HAy})_{1N} \\ (\alpha_{HAy})_{21} & .. & .. & (\alpha_{HAy})_{2N} \\ \vdots & \vdots & \vdots & \vdots \\ (\alpha_{HAy})_{M1} & .. & .. & (\alpha_{HAy})_{MN} \end{bmatrix} \begin{bmatrix} I_{ey}(\vec{r}_1\,') \\ I_{ey}(\vec{r}_2\,') \\ \vdots \\ I_{ey}(\vec{r}_N\,') \end{bmatrix}$$

and

$$\left[H_{Ay}(\vec{r}_m)\right]_{m\times 1} = \left[\alpha_{HAy}\right]_{m\times n}\left[I_{ey}(\vec{r}_n\,')\right]_{n\times 1}$$

$$(\alpha_{HAx})_{mn} = -(\alpha_{HAy})_{mn} = (\frac{1}{r_{mn}^{\ 2}} + \frac{j\beta}{r_{mn}})(\frac{l}{4\pi r_{mn}})(z - z_0)\exp(-jkr_{mn})$$

For z component of the magnetic field:

$$\left[H_{Az}(\vec{r}_m)\right]_{m\times 1} = \left[\alpha_{HAz1}\right]_{m\times n}\left[I_{ex}(\vec{r}_n\,')\right]_{n\times 1} + \left[\alpha_{HAz2}\right]_{m\times n}\left[I_{ey}(\vec{r}_n\,')\right]_{n\times 1}$$

$$(\alpha_{HAz1})_{mn} = (\frac{1}{r_{mn}^{\ 2}} + \frac{j\beta}{r_{mn}})(\frac{l}{4\pi r_{mn}})(x_m - x_0)\exp(-jkr_{mn})$$

$$(\alpha_{HAz2})_{mn} = (\frac{1}{r_{mn}^{\ 2}} + \frac{j\beta}{r_{mn}})(\frac{l}{4\pi r_{mn}})(y_m - y_0)\exp(-jkr_{mn})$$

BIBLIOGRAPHY

[1] Y. Vives-Gilavert, C. Arcambal, A. Loius, F. Daran, P. Eudeline and B. Mazari "Modeling Magnetic Radiations of Electronic Circuits Using Near-Field Scanning Method, " IEEE transactions on Electromagnetic Compatibility, Vol. 49, No3, August 2007.

[2] P. Fernandez-Lopez, C. Arcambal, D. Baudry, S. Verdeyme. B. Marzari, "Radiation Modeling and Electromagnetic Simulation of an Active Circuit" EMC Compo 09.

[3] Haixiao Weng "Prediction of Radiated Emission Using Near-field Measurements," PhD Dissertation Presented to the Faculty of the Graduate School of the University of Missouri-Rolla, 2006.

[4] Haixiao Weng; Beetner, D. G.; DuBroff, R.E; Jin Shi "Estimation of High-Frequency Currents From Near-Field Scan Measurements," IEEE transactions on Electromagnetic Compatibility, Vol. 49, Issue 4, Nov. 2007 Page(s):805 – 815.

[5] Constantine A Balanis "Antenna Theory," Third Edition, Page(s): 133-139, 2005.

[6] Constantine A Balanis "Antenna Theory," Third Edition, Page(s): 149, 2005.

[7] Jiang Xiao; David J. Pommerenke "Characterization of black holder PCB probes for EMI testing," MST EMC Lab Internal Report, May, 2009

[8] Jiang Xiao "Probe factor calculations method," MST EMC Lab Internal Report, May, 2009

VITA

Weiping He was born on January 22, 1978, in Zhuji, Zhejiang Province, China. She received her Bachelor's degree in Mechatronics Engineering in 2000 from Yanshan University and a Law degree in Intellectual Property in 2002, Renmin University of China, Beijing, China.

In January 2007, she began pursuing master's degree in the Electromagnetic Compatibility Laboratory at Missouri University of Science and Technology. She passed the thesis defense in December 2009 and received master's degree in May 2010.